USGS-OFR-82-409

UNITED STATES
DEPARTMENT OF THE INTERIOR
GEOLOGICAL SURVEY

THREE-DIMENSIONAL MODELING OF THE NEVADA TEST SITE AND VICINITY FROM TELESEISMIC P-WAVE RESIDUALS

By

Mary E. Monfort
John R. Evans

Open-file Report 82-409
1982

CONTENTS

ILLUSTRATIONS

ILLUSTRATIONS (continued)

TABLES

TABLES (continued)

ABSTRACT

A teleseismic P-wave travel-time residual study is described which reveals the regional compressional-velocity structure of southern Nevada and neighboring parts of California to a depth of 280 km. During 1980, 98 teleseismic events were recorded at as many as 53 sites in this area. P-wave residuals were calculated relative to a network-wide average residual for each event and are displayed on maps of the stations for each of four event-azimuth quadrants. Fluctuations in these map-patterns of residuals with approach azimuth combined with results of linear, three-dimensional inversions of some 2887 residuals indicate the following characteristics of the velocity structure of the southern Nevada region: 1) a low-velocity body exists in the upper crust 50 km northeast of Beatty, Nevada, near the Miocene Timber Mountain-Silent Canyon caldera complex. Another highly-localized low-velocity anomaly occurs near the southwest corner of the Nevada Test Site (NTS). These two anomalies seem to be part of a low-velocity trough extending from Death Valley, California, to about 50 km north of NTS. 2) There is a high-velocity body in the mantle between 81 and 131 km deep centered about 10 km north of the edge of the Timber Mountain caldera, 3) a broad low-velocity body is delineated between 81 and 131 km deep centered about 30 km north of Las Vegas, 4) there is a monotonic increase in travel-time delays from west to east across the region, probably indicating an eastward decrease in velocity, and lower than average velocities in southeastern Nevada below 31 km, and 5) considerable complexity in three-dimensional velocity structure exists in this part of the southern Great Basin.

Inversions of teleseismic P-wave travel-time residuals were also performed on data from 12 seismometers in the immediate vicinity of the Nevada Test Site

to make good use of the closer station spacing in that area. Results of these inversions show more details of the velocity structure but generally the same features as those found in the regional study.

INTRODUCTION

As part of the investigations of a possible site for a nuclear waste disposal area in the vicinity of the Nevada Test Site (NTS) a large-scale teleseismic P-wave relative-residual study has been undertaken. This study supplies constraints on compressional-velocity structure to depths of at least 280 km, and, in particular, provides information on the extent of any existing large magma bodies in the vicinity of NTS. Detailed examination of upper-crustal velocity structure directly under the proposed Yucca Mountain disposal site with these data is precluded by the large station spacing of the available seismic array. However, the data provide evidence of large-scale regional complexity in crustal structure in the vicinity of Yucca Mountain.

This report presents teleseismic P-delay data for the southern Nevada-southeastern California seismic array operated by A. M. Rogers of the U. S. Geological Survey for DOE/NV. We also present three-dimensional damped-least-squares inversions of these data. Tectonic interpretations of these results are left for later papers.

DATA ANALYSIS

During 1980, numerous teleseisms were recorded by the southern Nevada and southeastern California seismic network operated by the U.S. Geological Survey (Figure 1 and Table 1). This network used 1 Hz vertical-component L4-C^{TM} geophones to detect seismic signals. Amplified, frequency-modulated signals from the geophones are transmitted by radio and telephone lines to Golden, Colorado where they are recorded on Develocorder^{TM} film strips. Paper copies were made of the largest teleseisms occurring during 1980, generally those with magnitudes greater than 5.0. The waveforms of P or PKIKP phases were correlated for the first few cycles at each receiver using the methods

described by Iyer and others (1981) and Steeples and Iyer (1976). Correlatable troughs or peaks were timed for each event to an average accuracy of ±0.1 s.

Hypocentral information for the selected events was obtained from the Preliminary Determination of Epicenters, a regular publication of the National Earthquake Information Service, U. S. Geological Survey. The travel-time tables of Herrin (1968) were used to calculate the expected arrival time at each receiver, and the difference between the observed arrival time and this predicted arrival time were calculated for each station, producing travel-time residuals. Finally, a network-wide average residual for each event is determined and subtracted from every station's residual for that event to yield relative residuals. This relative-residual technique reduces effects of errors in hypocentral locations and of anomalies outside the volume under the seismic network. An event average was used for the reference in this study rather than a reference station because the network has no station outside the Basin and Range Province or in an area of known uniformity. Raikes (1980) provides a detailed discussion of the effects of event mislocations and velocity structure outside the volume under the array.

The final data set consists of 98 teleseisms including 90 P arrivals from distances of 25°-97° and eight PKIKP arrivals from 111°-152° distance. Divided into four azimuth quadrants, there were 11 earthquakes from an azimuth of 3°-81°, 26 from 121°-171°, 24 from 204°-267°, and 37 from 282°-351° (Tables 2, 3, 4, and 5).

A subset of these data, the group of observations from Nevada stations only, was compared to the full set. The restricted data set eliminated 12 seismometers situated southwest of the northern Death Valley-Furnace Creek fault zone (Figure 2). Residuals for both data sets were calculated and

plotted as contour maps for each of the four quadrants of approach azimuth and as an average for all azimuths (Figures 3a-e and 4a-e, Tables 6 and 7).

In a simple model of the uppermost crust longer ray paths to the high-elevation stations might produce relative delays having nothing to do with velocity anomalies under those stations. However, a plot of station elevation versus average relative residual for all azimuths together (Figure 5) shows no strong correlation between the two variables. Expected altitude effects for widely different velocities fit equally well.

Comparing a station elevation contour map (Figure 6) to an average travel-time residual map (Figure 3e) also shows a poor residual-elevation correlation. The only similar feature between the two maps shows an inverse correlation: the two lobes of negative residuals in California are regions of high elevation.

Wesson and others (1973) suggest that altitude effects are mitigated by the presence of relatively high-velocity materials at most high-altitude stations. Evans (1982) showed that whatever such effects exist are correctly assigned to the surface layer by the inversion. Therefore, no elevation corrections were made to these data.

Results:

Examining the results from both the total data set (Figures 3a-e) and the one including only the Nevada stations (Figures 4a-e) one sees few differences. The gross features of the two data sets are identical: a monotonic increase in travel time from west to east, a low-velocity zone at station EPN and higher velocities between NTS and Goldfield. The positive anomaly associated with EPN does not shift with changing event azimuth and is therefore probably due to a shallow crustal feature. The total variation in travel-time residuals across the array is about 0.8 s.

Two profiles of stations, one extending northwest-southeast and the other northeast-southwest were constructed as another method of searching for azimuth-dependent relative-residual patterns. All stations falling within 10 km of the lines in Figure 7a were projected onto those lines and their average relative-residuals for appropriate azimuth ranges were plotted (Figure 7b). Station EPN on the northwest-southeast section is associated with positive residuals for both azimuths, verifying the existence of a shallow low-velocity body there. On both profiles the reversal of the overall shape of the curves with reversal of event azimuth does suggest the presence of a broad high-velocity body in the upper mantle beneath NTS. The inversion results discussed below verify both these interpretations (cf. Figures 10b and 11c).

INVERSION TECHNIQUE

The data were also analyzed in a three-dimensional linear inversion utilizing the Aki-Christofferson-Husebye (ACH) damped-least-squares technique. For a complete discussion of this inversion method the reader is referred to Aki and others (1977), Ellsworth and Koyanagi (1977), and Romanowicz (1979). A cursory explanation follows.

In the ACH technique, an initial velocity model is assigned to the region under the array. This model consists of plane parallel layers with constant layer velocity and is used mainly for initial ray tracing. The choice of initial model is not critical since differences between reasonable models produce only second-order effects on ray location (Aki and others, 1977).

Each layer is then divided into right rectangular blocks, and appropriate segments of these rays are allocated to the blocks through which the rays pass. Tracing all rays for all events through the initial model produces a dense network of rays in the modeled volume under the array. Since rays come

to each station from several directions and since rays pass through each block in several directions on their way to several different stations, it is possible to invert relative-residual data to find the velocity perturbations of each block. The ACH technique uses a damped-least-squares inversion to find these block velocity perturbations.

The inversion's ability to isolate (resolve) the velocity perturbation of any block depends on having enough rays in that block with good "cross-fire" of rays. That is, not all rays should pass through the block in the same direction. Therefore, blocks with fewer than 10 rays are not modeled and it is important to recognize that resolution varies from place to place within the model.

The resulting isolation of a block is quantitatively given by a resolution matrix which the inversion generates, along with the velocity perturbation model and standard error estimates, for each block. The diagonal element of the resolution matrix generally indicates how much of that block's velocity perturbation is actually due to velocity anomalies in that part of the earth. This diagonal element will be called "the resolution" and should ideally be near unity. Off-diagonal elements of the resolution matrix indicate which other blocks contribute to the velocity perturbation and by how much. Thus, the resolution matrix is like a translucent lens through which the real velocity structure is viewed; the velocity model produced by the inversion equals the "true" model multiplied by the resolution matrix.

Resolution and standard errors can be combined in a "figure-of-merit" to describe the minimum credible velocity perturbation in well resolved, smoothly-varying models. This figure-of-merit is empirically defined to range from two times the standard error for resolution of 0.8 to three or four times the

standard error for a resolution of 0.6 (Evans, 1982). Thus a block with a standard error of 0.3 and a resolution of 0.8 is thought to reliably resolve velocity perturbations larger than ±0.6% while the same standard error in a block with resolution of 0.6 implies uncertainty in any velocity perturbation less than about ±1.2%. Velocities in blocks with resolution less than about 0.6 can only be considered averages of velocities in several surrounding blocks, with those averages quantitatively described by columns of the resolution matrix.

To generate a mathematically unique velocity perturbation model a "damping parameter" must be introduced. Large damping parameters greatly smooth the model, removing detail and reducing velocity perturbations but giving small standard errors. Small damping parameters allow large variations between neighboring blocks and good resolution but large standard errors. We empirically chose a damping parameter of 0.0030 $s^2/\%^2$. This value was large enough to provide a stable solution and small enough for good resolution. The effects of larger and smaller damping parameters is shown in Table 8.

Block dimensions chosen for the inversion are constrained by the station spacing and other factors. Ideally the height of the blocks should be approximately 1.5 times the horizontal dimension (Aki and others, 1977) since teleseisms' steep incidence angles (within 30° of vertical at the earth's surface) provide better horizontal than vertical resolution. However, our 35 km average station spacing (20 km for the NTS region) precludes this block proportion if we wish to model crustal layers. Our use of wider blocks results in horizontal smoothing of the velocity perturbations and only fair resolution between vertically adjacent blocks. The NTS data set shows more horizontal detail because of the smaller block horizontal dimensions.

Results of the inversion were so similar for the data set restricted to Nevada and for the whole data set that the restricted data inversion will not be discussed. Because of the smaller station spacing in the immediate vicinity of the Nevada Test Site we will discuss a third series of models generated using smaller blocks and data from only 12 stations in and around the Test Site (Table 1 and Figure 8).

Initial velocity models are shown in Tables 9 and 10; resulting velocity perturbations, resolution, and standard errors for upper-crustal layers of models nov9b and nov9e can be seen in Tables 11 and 12.

Combining the two crustal layers into one had little affect on the pattern of velocity variations in the mantle layers, verifying the inversion's success in separating crustal from mantle effects. Increasing block size or shifting the block boundaries (these boundaries strictly speaking are ad-hoc artificial constraints on the models) half a block northwest also had little affect, substantiating the stability of the final models.

Velocity perturbations are given as $\Delta v/v$ where v is the average layer velocity. Due to the use of relative residuals, this average velocity does not correspond to any known absolute velocity in the layer--the technique detects velocity variations within layers but does not produce absolute velocity information. Therefore velocity contrasts and total velocity variation in a layer are the useful features of the velocity perturbation model.

The inversion technique provides two ways of modeling the top layer which are both included here for comparison. The first method divides the top layer into rectangular blocks just like all the other layers, while the second method computes a perturbation in velocity for each station. These station

velocity perturbations correspond to station correction terms for shallow velocity structure.

The variance improvement, that is the fraction of the original relative-residual data which could be explained by the model result, was in the lower- to mid-80 percentile. Approximately 15% of the data cannot be explained by the final velocity models and must be due to reading errors and to velocity structure on a scale too fine to be resolved in the large blocks used. Other studies known to the authors also achieve variance improvements less than about 90% (Stauber, 1982; Oppenheimer and Herkenhoff, 1981).

RESULTS

Regional:

Upper-crustal models from the three-dimensional linear inversion show velocity variations of as much as 6% from the mean layer velocity in the upper 15 km (Figures 9 and 11a). A low-velocity body under station EPN is evident ($\Delta v/v = -6\%$) as is a low-velocity body in the vicinity of Caliente ($\Delta v/v = -4\%$). Otherwise there is not much correlation between these velocities shown in Figures 9 and 11a and the pattern of average residuals in Figure 3. The two most obvious differences are a velocity perturbation of -4% at LSM (southwestern NTS) and the absence of a well-developed regional west-to-east decrease in velocity in this crustal layer. These dissimilarities may be due to the restriction of the inversion to the upper 15 km whereas the average travel-time residuals, while reflecting the effects of shallow structure, do not represent as well defined a depth interval.

Station EPN shows the effects of low velocities in Figures 3, 9, and 11a. The two ways the inversion can model the upper layer yield similar patterns of velocity perturbations (Figures 9 and 11a) with maxima and minima occurring in

the same regions. The figure-of-merit indicates that these perturbations are well resolved in both upper layer models.

In the lower half of the crust (Figures 10a and 11b) are poorly resolved velocity perturbations of much lower magnitude. The largest perturbations in this layer also are in the least resolved blocks found at the periphery of the model (where most rays are subparallel to one another and ray cross-fire is minimal). Hence, less significant velocity structure is seen in this layer than in the upper crust. A significantly high-velocity block does exist just east of Yucca Mountain in Figures 10a and 11b as well as just north of the Mountain in Figure 11b.

Layer 3 covers the uppermost mantle from 31 km to 81 km and should include the asthenospheric lid (at 65 km depth) described by Chapman and Priestly (1980). The resolution in this layer is very good and velocity perturbations vary from -2.8% to 3.9% (Figures 10b and 11c). A trend of increasing velocity to the west is apparent, while no significant perturbations occur beneath the crustal low-velocity bodies associated with EPN and Caliente.

Layer 4 includes asthenospheric mantle and ranges from 81 km to 131 km deep. It shows a large high-velocity zone north-northwest of the center of the model, station BGB, with more than 6000 km^2 between about 3% and 4.5% faster than the average layer velocity (Figures 10c and 11d). In addition, there is a well-resolved low-velocity body (-4%) southeast of APK. This low-velocity body does not appear in any other layer.

Layer 5 extends from 131 km to 231 km (Figures 10d and 11e) and has only two blocks with velocity perturbations greater than 3%. Both these blocks are in the extreme north. Average perturbations are approximately $\pm$1%. A northeast-southwest striking regional velocity gradient is seen, but the mantle appears relatively homogeneous at this depth.

Nevada Test Site:

The data set restricted to the Nevada Test Site shows a relative high-velocity body under and west of BGB in the upper layer of model nts9b (Figure 12). The volume under EPN exhibits a lower velocity with a contrast of 5.5% between the upper crustal velocities associated with the two stations. This velocity contrast is about the same as that found in the regional study.

In deeper layers (Figures 13a-d) the velocity perturbations under Pahute Mesa are positive and more pronounced north of station EPN, attaining values as high as 3% at depths of 81 km to 231 km (where the figure-of-merit verifies anomalies greater than about 1.5%). Spence (1974) found a high-velocity body at approximately 45 km to 180 km depth in this same region using teleseismic residuals and reversed source to receiver geometry. Minster and others (1981) also used reversed teleseismic source-receiver geometry to resolve a high-velocity body under Pahute Mesa extending to greater than 100 km depth and shifting to the north with increasing depth.

Yucca Mountain has no pronounced velocity perturbation associated with it at any depth or for any model. The current data cannot resolve the upper crust beneath the mountain.

CONCLUSIONS

This study of the southern Great Basin has yielded some interesting results. There is a low-velocity upper-crustal body in the vicinity of Pahute Mesa and the Timber Mountain caldera (station EPN), underlain by a high-velocity mantle body between 81 km and 131 km deep. A northwest to southeast trend of decreasing velocity exists in the mantle, and is obvious on the travel-time contour plots.

Due to the large station spacing of available data, anomalous bodies with lateral dimensions less than 35 km may have gone undetected, but, within that

limitation, no major mantle low-velocity body is seen. No upper-crustal data are available for the Yucca Mountain disposal site itself.

ACKNOWLEDGMENTS

The authors would like to thank H. M. Iyer for his guidance and patience; Mary Lou Zoback for her exceptionally thoughtful and helpful review of this manuscript and pellucid discussions of Basin and Range tectonics; Al Rogers and Steve Harmsen for supplying films and help at Golden, Colorado; and Doug Stauber and Tim Hitchcock for additional reviews.

REFERENCES

Aki, K., A. Christofferson, and E.S. Husebye, 1977. Determination of the three-dimensional seismic structure of the lithosphere, J. Geophys. Res., v. 82, pp. 277-296.

Chapman, D.S. and K. Priestley, 1980. Detailed seismic characterization of geothermal subprovinces in central Nevada, Geothermal Research Program, Final Report to the U. S. Geological Survey.

Eaton, G.P., R.R. Wohl, H.J. Prostka, D.R. Mabey, and M.D. Kleinkopf, 1978. Regional gravity and tectonic patterns: their relation to late Cenozoic epeirogeny and lateral spreading in the western Cordillera, in Geol. Soc. Am. Memoir 152, Cenozoic Tectonics and Regional Geophysics of the Western Cordillera, edited by R.B. Smith and G.P. Eaton, Geol. Soc. Am., Boulder, Colorado, pp. 51-93.

Ellsworth, W.L. and R.Y. Koyanagi, 1977. Three-dimensional crust and mantle structure of Kilauea Volcano, Hawaii, J. Geophys. Res., v. 82, pp. 5379-5394.

Evans, J.R., 1982. Compressional-wave velocity structure of the upper 350 km under the eastern Snake River Plain near Rexburg, Idaho, J. Geophys. Res., in press.

Herrin, E. (ed.), 1968. 1968 Seismological tables for P phases, Seis. Soc. Am., Bulletin, v. 58, no. 4.

Hoover, D.L., W.C. Swadley and A.J. Gordon, 1981. Correlation characteristics of surficial deposits with a description of surficial stratigraphy in the Nevada Test Site region, U.S. Geological Survey Open-File Report 81-512.

Iyer, H.M., J.R. Evans, G. Zandt, R.M. Stewart, J. Coakley and J. Roloff, 1981. A deep magma body under the Yellowstone caldera: delineation using

teleseismic P-wave residuals and tectonic interpretation, Geol. Soc. Am. Bulletin, Part II v. 92, pp. 1471-1646.

Minster, J.B., J.M. Savino, W.L. Rodi, J.F. Masso and T.H. Jordan, 1981. Three-dimensional velocity structure of the crust and upper mantle beneath the Nevada Test Site (Abs.), EOS, Trans., Am. Geophys. Un., v. 62, p. 972.

Oppenheimer, D.H. and K.E. Herkenhoff, 1981. Velocity-density properties of the lithosphere from three-dimensional modeling at the Geysers-Clear Lake region, California, J. Geophys. Res., v. 86, pp. 6057-6065.

Raikes, S.A., 1980. Regional variations in upper mantle structure beneath southern California, Geophys. J. R. Astr. Soc., v. 63, pp. 187-216.

Romanowicz, B.A., 1979. Seismic structure of the upper mantle beneath the United States by three-dimensional inversion of body wave arrival times, Geophys. J. R. Astr. Soc., v. 57, pp. 479-506.

Spence, W., 1974. P-wave residual differences and inferences on an upper mantle source for the Silent Canyon volcanic center, Southern Great Basin, Nevada, Geophys. J. R. Astr. Soc., v. 38, pp. 505-523.

Stauber, D.A., 1982. Two-dimensional compressional wave velocity structure for a profile through the San Francisco Peaks volcanic field, Arizona, from teleseismic P-residual measurements, J. Geophys. Res., in press.

Steeples, D.W. and H.M. Iyer, 1976. Low-velocity zone under Long Valley as determined from teleseismic events, J. Geophys. Res., v. 81, pp. 849-860.

Stewart, J.H., 1978. Basin-range structure in western North America: a review, in Geol. Soc. Am. Memoir 152, Cenozoic Tectonics and Regional Geophysics of the Western Cordillera, edited by R.B. Smith and G.P. Eaton, Geol. Soc. Am., Boulder, Colorado, pp. 1-33.

Wesson, R.L., J.C. Roller and W.H.K. Lee, 1973. Time-term analysis and geologic interpretation of seismic travel-time data from the Coast Ranges of central California, Seis. Soc. Am., Bulletin, v. 63, pp. 1447-1471.

TABLE 1
Station Coordinates

	Station		Latitude (° ' North)		Longitude (° ' West)		Elevation (meters)
*	AMR	Amargosa	36	23.86	116	28.45	720
	APK	Angels Peak	36	19.17	115	34.46	2680
&	BGB	Big Butte	37	02.27	116	13.66	1720
	BLT	Belted Range	37	28.93	116	07.35	1820
&	BMT	Black Mountain	37	17.02	116	38.74	2190
	BRO	Bare Mountain	36	45.76	116	37.52	920
&	CDH1	Calico Hills	36	51.62	116	19.05	1387
&	CPX	CP-1, Nevada	36	55.80	116	03.30	1285
	CTS	Cactus Peak	37	39.40	116	43.54	1890
	DLM	Delamar Mountain	37	36.35	114	44.33	1730
&	EPN	Echo Peak	37	12.85	116	19.42	2285
	EPR	E. Pahranagat Range	37	10.12	115	11.19	1300
*	FMT	Funeral Mountains	36	38.38	116	46.73	1025
&	GLR	Groom Lake Road	37	11.96	116	01.06	1435
	GMN	Gold Mountain	37	18.01	117	15.58	2155
	GMR	Groom Range	37	20.03	115	46.27	1580
*	GVN	Grapevine	37	00.09	117	20.55	1190
*	GWV	Greenwater Valley	36	11.20	116	40.24	1540
	JON	Johnnie	36	26.39	116	06.18	920
	KRN	Kawich Range	37	42.37	116	20.07	2570
	KRNA	Kawich Range	37	44.47	116	22.75	1980
*	LCH	Last Chance Range	37	14.08	117	38.84	1455
&	LOP	Lookout Peak	36	51.25	116	10.05	1695
&	LSM	Little Skull Mtn.	36	44.40	116	16.37	1140
*	MCA	Marble Canyon	36	38.89	117	16.85	300
	MCX	Mercury	36	39.37	115	59.45	1160
&	MCY	Mercury	36	39.70	115	57.73	1285
	MGM	Magruder Mountain	37	26.47	117	29.79	2100
	MTI	Mount Irish	37	40.60	115	16.36	1525
	MZP	Montezuma Peak	37	42.04	117	22.98	2375
	NEL	Nelson	35	42.73	114	50.62	1052
	NMN	Nasa Mountain	37	04.85	116	49.09	1500
*	NOP	Nopah Range	36	07.68	116	09.16	970
	NPN	North Pahroc Range	37	39.16	114	56.22	1650
*	PGE	Panamint Range	36	20.93	117	03.95	1850
*	PPK	Piper Mountain	37	25.58	117	54.43	1830
	PRN	Pahroc Range	37	24.42	115	02.99	1470
	QCS	Queen City Summit	37	46.07	115	54.98	1890
*	QSM	Queen of Sheba Mine	35	57.93	116	52.10	670
	RVE	Reveille Range	38	01.18	116	11.51	2290
	SDH	Striped Hills	36	38.73	116	20.29	1055
	SGV	S. Grapevive Mtn.	36	58.87	117	01.94	1565
	SHRG	Sheep Range	36	30.27	115	09.31	1645
&	SPRG	Spotted Range	36	41.64	115	48.56	1235

TABLE 1 (continued)
Station Coordinates

	Station		Latitude (° ' North)		Longitude (° ' West)		Elevation (meters)
	SRG	Seaman Range	37	52.93	115	04.08	1645
&	SSP	Shoshone Peak	36	55.50	116	13.11	2065
	SVP	Silver Peak Range	37	42.90	117	48.05	2620
*	TMO	Tin Mountain	36	48.32	117	24.48	2195
	TNP	Tonopah	38	04.92	117	13.08	1931
	TPK	Tolicha Peak	37	16.11	116	48.26	2080
	TPU	Tempiute Mountain	37	36.30	115	38.95	1915
	WRN	Worthington Mtn.	37	58.90	115	35.30	1760

* Stations used only in the California-Nevada joint data set.
& Stations used in the NTS inversions.

TABLE 2
Hypocentral data for events from the northeast quadrant.

Name	Date m/d/y	Origin Time h:m:s	Latitude (° ' N)		Longitude (° ' W)		Depth (km)	m_b	Location	Delta* (°)	Back Azimuth* (° from N)
01p2	01/01/80	16:42:40.0	38	48.9	27	46.8	10	6.1	Azores	67	58
54p1	03/26/80	20:43:37.9	23	52.0	45	33.5	10	6.0	N. Atlantic Ridge	61	81
04p2	05/28/80	19:51:19.3	38	28.9	-14	15.1	14	5.6	Sicily	92	37
07p1	07/09/80	02:11:52.8	39	16.1	-23	02.5	14	5.8	Aegean Sea	95	31
92t2	08/12/80	12:11:44.4	64	43.4	17	14.9	10	5.3	Iceland	61	29
09t1	10/10/80	12:25:23.5	36	11.7	-1	21.2	10	6.3	Algeria	87	46
10t1	10/10/80	12:37:09.7	36	21.8	-1	37.9	10	5.7	Algeria	87	46
11t1	10/10/80	15:39:09.8	36	13.3	-1	36.7	10	6.0	Algeria	87	46
12t1	10/11/80	07:09:57.0	73	21.2	-54	59.8	1	5.7	Novaya Zemlya	70	3
13t3	11/23/80	18:34:53.8	40	54.8	-15	22.0	10	6.1	southern Italy	91	35
15t3	12/07/80	17:37:09.7	36	01.6	-1	13.7	10	5.4	Algeria	87	46

* from station BGB.

TABLE 3
Hypocentral data for events from the southeast quadrant.

Name	Date m/d/y	Origin Time h:m:s	Latitude (° ' N)		Longitude (° ' W)		Depth (km)	m_b	Location	Delta* (°)	Back Azimuth* (° from N)
21t1	01/14/80	21:51:01.8	-33	11.6	69	27.5	14	5.6	Chile-Argentina	82	142
22p1	01/16/80	15:49:15.0	-14	32.5	73	29.6	94	5.7	Peru	65	134
25t1	01/27/80	16:38:01.1	-35	22.7	105	52.1	10	5.6	Easter Island	73	171
27t1	02/04/80	00:56:07.2	5	26.2	82	39.1	10	5.6	Southern Panama	44	127
28p1	02/04/80	03:45:56.0	-57	54.4	7	11.3	10	5.9	SW Atlantic	130	139
46p1	03/07/80	08:25:07.8	-16	41.3	72	57.1	43	5.4	near Peru	67	135
57p1	03/29/80	06:41:50.5	-43	04.7	75	12.2	33	5.6	off S. Chile	88	151
75t1	05/02/80	19:09:06.4	-24	19.5	67	02.0	157	5.4	Chile-Argentina	77	135
79t1	05/26/80	18:41:36.8	-19	21.4	69	17.2	62	6.0	northern Chile	71	133
83p2	06/21/80	20:19:26.4	-57	58.4	10	39.4	10	6.0	SW Atlantic	128	139
84p2	06/25/80	12:04:56.9	4	26.2	75	46.7	162	5.7	Colombia	49	121
06ap1	07/13/80	06:20:30.3	-33	28.4	70	09.1	103	5.6	Chile-Argentina	82	143
05at1	07/14/80	10:03:23.0	11	03.4	85	30.9	96	4.8	Nicaragua	38	125
02at1	07/19/80	11:52:20.6	-28	59.8	69	40.5	110	6.1	Chile-Argentina	79	140
01ap1	07/30/80	06:56:16.7	5	16.6	82	39.9	10	5.8	south of Panama	44	128
90t1	08/03/80	03:00:49.7	-35	15.1	69	59.5	151	5.4	Argentina	84	144
91t3	08/09/80	05:45:09.5	15	53.3	88	31.0	22	5.9	Honduras	32	123
93p1	08/18/80	15:07:52.6	-1	56.9	80	01.0	55	5.6	off Ecuador coast	51	131
95p1	09/03/80	22:12:39.1	3	14.3	78	11.4	33	5.7	southern Panama	48	125
100t1	09/28/80	14:29:41.5	-55	58.4	27	34.4	96	5.9	S Sandwich Island	119	140
101t1	10/08/80	22:01:34.8	-1	22.8	77	41.2	190	5.5	Ecuador	52	128
102t1	10/24/80	14:53:35.1	18	12.7	98	14.4	72	6.4	central Mexico	25	135
104t3	11/04/80	16:21:15.3	13	51.7	90	55.6	83	5.4	Guatemala	32	129
107p1	11/10/80	16:24:40.5	-31	34.6	67	28.1	21	5.6	Argentina	82	140
108p1	11/11/80	10:36:58.2	-51	25.3	-28	47.8	10	6.2	south of Africa	151	131
14at1	11/23/80	23:40:29.8	4	48.3	76	13.0	108	6.4	Colombia	49	121

* from station BGB.

TABLE 4
Hypocentral data for events from the southwest quadrant.

Name	Date m/d/y	Origin Time h:m:s	Latitude (° ' N)		Longitude (° ' W)		Depth (km)	m_b	Location	Delta* (°)	Back Azimuth* (° from N)
26p3	02/03/80	11:58:39.8	-17	38.9	171	11.0	33	6.2	Tonga	75	234
35p1	02/12/80	03:20:23.2	-4	42.2	-153	11.8	75	6.0	New Ireland	93	267
30p1	02/22/80	21:15:42.1	-10	41.6	-161	36.1	68	5.9	Solomon Islands	90	257
47t2	03/08/80	22:12:10.3	-22	40.4	-171	21.4	38	6.0	Loyalty Islands	90	242
50t1	03/23/80	19:36:58.4	-21	52.7	139	01.2	1	5.7	Tuamoto (blast)	62	204
66t1	05/12/80	16:37:36.9	-14	26.2	-167	50.0	33	6.0	New Hebrides	88	250
29t1	05/14/80	11:26:00.6	-6	00.4	-154	30.8	57	6.1	Solomon Islands	93	265
12at1	06/18/80	10:49:10.0	-15	16.1	173	34.2	43	5.9	Tonga	75	237
37t1	06/19/80	08:31:38.7	-29	57.4	-177	59.2	51	6.2	Kermadec	91	232
10at1	06/23/80	20:13:20.9	-28	46.6	176	41.2	49	5.6	Kermadec	87	230
09at1	06/25/80	23:18:20.4	-5	14.0	-151	41.2	49	6.2	New Britan region	95	267
38t5	07/14/80	16:15:01.7	-29	16.4	177	09.2	49	6.1	Kermadec	87	230
60p3	07/17/80	19:42:26.2	-12	39.8	-166	00.7	56	6.0	Santa Cruz Islands	88	253
04ap1	07/20/80	21:20:03.9	-17	51.9	178	37.5	591	6.0	Fiji	80	239
61p2	07/21/80	21:20:23.1	-12	13.5	-166	29.0	60	6.1	Santa Cruz Islands	87	253
03at1	07/22/80	07:06:23.0	-20	18.1	-169	36.4	122	6.1	Vanuatu Islands	90	245
65p3	07/29/80	03:11:56.3	-13	06.1	-166	20.3	48	5.9	New Hebrides	88	252
98p1	09/26/80	17:28:15.4	-15	01.7	-167	17.7	116	5.8	Vanuatu Islands	88	250
48p2	10/25/80	07:00:07.9	-21	58.9	-170	01.5	33	6.0	Loyalty Islands	91	243
49p2	10/25/80	11:00:05.1	-21	53.4	-169	51.2	33	5.8	Loyalty Islands	91	243
39p1	10/28/80	02:38:10.0	-30	27.8	177	56.4	33	5.9	Kermadec	89	230
44p1	11/30/80	12:24:39.8	-19	25.6	175	51.0	202	6.0	Tonga	79	236
51t1	12/03/80	17:32:58.2	-21	56.3	138	57.7	1	5.7	Tuamoto	62	204
45t1	12/15/80	08:12:45.4	-17	35.6	172	18.0	33	6.2	Tonga	76	235

* from station BGB

TABLE 5
Hypocentral data for events from the northwest quadrant.

Name	Date m/d/y	Origin Time h:m:s	Latitude (° ' N)	Longitude (° ' W)	Depth (km)	m_b	Location	Delta* (°)	Back Azimuth* (° from N)
13at1	01/07/80	20:06:57.3	51 19.4	-156 40.3	112	5.6	Kamchatka	61	314
20p1	01/12/80	15:57:01.9	41 40.7	-143 35.3	33	5.7	Japan	73	310
23t2	01/19/80	07:02:35.0	51 19.0	178 29.3	50	5.8	Aleutians	46	309
24t1	01/23/80	08:12:26.7	52 17.2	-160 19.1	33	5.7	off Kamchatka	58	314
32p3	02/23/80	05:51:03.2	43 31.8	-146 45.2	44	6.4	Kuril Islands	70	310
33t1	02/23/80	22:38:53.5	43 14.6	-146 54.0	45	5.9	Kuril Islands	70	310
34p1	02/27/80	12:44:26.7	43 16.1	-146 50.7	42	5.9	Kuril Islands	70	310
42p1	03/02/80	23:28:57.1	26 59.6	-126 37.3	33	5.7	East China Sea	93	307
52t1	03/24/80	03:59:51.3	52 58.1	167 40.2	33	6.3	Aleutians	39	311
118p1	03/24/80	04:41:59.1	52 53.2	167 42.8	33	6.1	Aleutians	39	311
58t1	03/31/80	07:32:31.8	35 26.9	-135 28.4	359	5.9	Honshu, Japan	82	308
67t1	04/16/80	06:50:15.3	27 57.8	-140 06.8	260	5.4	Bonin Island	84	300
70t1	04/25/80	03:56:57.4	49 56.8	-78 48.5	1	5.5	USSR (blast)	92	350
53t1	05/03/80	09:30:10.3	51 09.2	-173 46.8	51	5.7	Aleutians	50	310
77t3	05/15/80	18:58:25.6	-6 13.9	-125 47.4	33	5.9	Banda Sea	116	282
71t1	05/22/80	03:56:57.7	49 45.5	-78 06.1	1	5.4	USSR (blast)	93	351
05p1	06/09/80	18:38:01.1	15 22.9	-147 29.9	23	5.7	Mariana Islands	86	286
116p1	06/09/80	20:06:35.0	40 47.8	-139 51.6	165	5.6	Honshu, Japan	76	311
08ap1	06/09/80	20:06:35.0	40 47.8	-139 51.6	165	5.6	Honshu, Japan	76	311
07at1	06/10/80	23:13:23.7	51 32.8	-150 38.6	543	5.2	Sea of Okhotsk	64	316
78p2	06/16/80	20:48:59.1	-7 24.7	-128 35.5	170	6.0	Banda Sea	114	280
11ap1	06/21/80	21:30:17.3	37 20.3	-134 57.0	368	5.0	Sea of Japan	81	310
72t1	06/29/80	02:32:57.7	49 55.2	-78 50.9	1	5.7	USSR (blast)	92	350
86p1	06/29/80	07:20:05.5	34 48.5	-139 10.9	15	5.8	Honshu, Japan	80	306
88p1	07/29/80	14:58:40.8	29 35.9	-81 05.5	18	6.1	Nepal	112	344
89t1	08/01/80	23:07:14.7	59 37.0	148 56.2	26	5.4	Kenai Peninsula	31	328
96t1	09/14/80	02:42:39.3	49 58.6	-78 53.3	1	6.2	USSR (blast)	92	350
87t2	09/24/80	17:54:24.1	35 27.0	-139 57.8	73	6.1	Honshu, Japan	79	306
103t1	11/01/80	04:40:36.8	14 22.0	-145 46.4	103	5.6	Mariana Islands	88	286
105t1	11/04/80	20:26:00.7	53 49.0	-160 44.5	33	5.9	Kamchatka	57	316
106p1	11/06/80	01:34:27.5	43 43.3	-86 05.5	33	5.5	China	97	344
109p1	11/19/80	19:00:46.9	27 23.6	-88 45.1	17	6.0	Sikkim	112	336
110p1	11/21/80	14:56:13.4	51 47.9	176 08.5	53	5.7	Aleutians	44	309
113p1	12/04/80	10:46:27.0	52 15.4	-160 57.0	33	5.6	Kamchatka	58	314
74t1	12/14/80	03:47:06.6	49 55.9	-79 00.3	1	5.9	USSR (blast)	92	350
68t1	12/16/80	13:08:24.4	28 28.5	-139 35.6	389	5.3	Bonin Island	84	301
117p1	12/19/80	23:32:41.9	30 34.9	-140 38.6	82	6.2	Honshu, Japan	82	302

* from station BGB

TABLE 6
Residuals for the complete data set

Station	NE	RMS/#	SE	RMS/#	SW	RMS/#	NW	RMS/#	AVE	#
AMR	.13	.20/09	-.23	.12/22	-.25	.08/22	-.17	.14/19	-.13	72
APK	.51	.10/06	.12	.14/19	.26	.09/14	.33	.21/21	.30	60
BGB	-.40	.11/08	-.02	.15/21	-.12	.08/24	-.18	.19/31	-.18	84
BLT	-.13	.22/10	-.01	.12/21	-.30	.07/22	-.04	.15/28	-.12	81
BMT	-.43	.18/08	-.13	.09/14	-.14	.12/14	.07	.13/19	-.16	55
BRO	-.19	.05/07	.06	.08/18	-.06	.08/22	-.13	.07/22	-.08	69
CDH1			.35	.25/03	.12	.30/05	-.18	.17/06	.10	14
CPX	.09	.21/04	.20	.17/16	-.05	.14/13	-.34	.09/17	-.03	50
CTS	-.35	.16/10	-.27	.10/20	-.15	.12/20	.14	.10/28	-.16	78
DLM	.20	.16/05	.09	.12/16	.41	.09/17	.12	.15/18	.21	56
EPN	-.09	.13/10	.28	.17/20	.23	.11/19	.22	.22/20	.16	69
EPR	.44	.17/10	.09	.18/23	.34	.16/20	.14	.14/34	.25	87
FMT	-.07	.14/04	.06	.08/17	-.04	.08/16	-.07	.12/18	-.03	55
GLR	-.24	.15/06	.07	.12/18	-.26	.08/19	-.26	.11/26	-.17	69
GMN	.16	.03/02	.03	.15/06	-.09	.10/06	.22	.11/17	.08	31
GMR	.07	.15/05	.14	.07/21	-.13	.10/13	-.11	.09/27	-.01	66
GVN	.02	.21/08	-.08	.09/17	-.06	.12/16	.13	.18/22	.00	63
GWV	.03	.28/04	-.42	.12/15	-.31	.07/18	-.14	.15/19	-.21	56
JON	.27	.16/09	-.09	.13/18	.14	.10/20	.02	.16/19	.08	66
KRN			.20	.11/03	.19	.04/02	.34	.07/04	.24	9
KRNA	-.16	.12/08	.07	.16/14	.04	.12/18	.08	.19/19	.01	59
LCH	-.04	.18/08	-.37	.12/14	-.26	.10/16	.12	.16/24	-.14	62
LOP	-.12	.30/09	.26	.09/24	.19	.09/24	-.20	.18/26	.03	83
LSM	-.20	.28/07	.21	.10/17	.28	.07/12	-.05	.14/15	.06	51
MCA	-.29	.14/07	-.45	.10/14	-.32	.14/22	-.31	.15/23	-.34	66
MCX			.15	/01	.18	/01	-.18	.10/02	.05	4
MCY	.26	.07/07	.07	.10/19	.16	.08/18	-.17	.18/23	.08	67
MGM	-.06	.15/07	-.21	.14/16	-.24	.10/13	.12	.10/21	-.10	57
MTI	.17	.21/06	.10	.10/16	-.02	.11/19	.05	.21/20	.08	61
MZP	-.25	.08/05	-.25	.15/13	-.19	.13/13	-.04	.06/16	-.18	47
NMN	-.53	.10/04	-.05	.09/16	-.20	.10/16	.04	.13/22	-.19	58
NOP	.20	.18/11	-.31	.14/21	-.12	.16/22	-.03	.17/24	-.07	78
NPN	.31	.22/06	.16	.11/15	.39	.11/20	.19	.11/21	.26	62
PGE	.15	.11/06	-.24	.13/15	-.02	.12/21	-.14	.12/15	-.06	57
PPK	.09	.15/07	-.04	.13/17	.14	.14/18	.37	.14/26	.14	68
PRN	.42	.18/10	.11	.15/20	.37	.10/18	.14	.13/29	.26	77
QCS	.01	.15/05	.19	.12/21	-.18	.10/18	.07	.11/17	.02	61
QSM	-.09	.22/04	-.60	.11/16	-.40	.11/18	-.29	.14/19	-.35	57
RVE	.06	.15/04	.08	.09/06	-.02	.10/04	-.09	.09/03	.01	17
SDH	.09	.06/07	.01	.08/17	.04	.08/20	-.12	.11/19	.01	63
SGV	-.24	.23/10	.03	.10/21	-.08	.14/19	.10	.17/27	-.05	77
SHRG	.25	.10/07	.02	.10/20	.31	.11/18	.20	.20/17	.20	62
SPRG	.32	.08/09	.10	.14/20	.23	.07/20	-.30	.18/23	.09	72
SRG	.13	.13/04	.21	.13/19	.23	.12/18	.19	.19/27	.19	68
SSP	-.25	.22/08	.19	.10/20	.10	.08/19	-.14	.21/19	-.03	66
SVP	-.10	.16/03	.09	.16/13	.16	.12/11	.21	.10/10	.09	37
TMO	.00	.13/02	.02	.08/13	.09	.08/18	.09	.17/20	.05	53

TABLE 6 (continued)
Residuals for the complete data set

Station	NE	RMS/#	SE	RMS/#	SW	RMS/#	NW	RMS/#	AVE	#
TNP	-.20	.09/05	.02	.18/13	.06	.17/09	.11	.16/16	.00	43
TPU	.07	.13/03	.10	.07/14	-.28	.11/17	-.12	.07/19	-.06	53
WRN	.00	/01	.13	.12/06	-.12	.05/05	.06	.11/08	.02	20

TABLE 7
Residuals for the Nevada data set

Station	NE	RMS/#	SE	RMS/#	SW	RMS/#	NW	RMS/#	AVE	#
APK	.52	.12/06	.05	.14/19	.21	.09/14	.32	.21/21	.28	60
BGB	-.38	.11/08	-.08	.13/21	-.17	.07/24	-.19	.16/31	-.21	84
BLT	-.12	.19/10	-.08	.11/21	-.35	.07/22	-.05	.14/28	-.15	81
BMT	-.42	.18/08	-.20	.09/14	-.19	.13/14	.07	.13/19	-.19	55
BRO	-.17	.06/07	-.01	.08/18	-.11	.08/22	-.13	.09/22	-.11	69
CDH1			.27	.23/03	.08	.29/05	-.19	.16/06	.05	14
CPX	.08	.18/04	.14	.16/16	-.10	.13/13	-.37	.09/17	-.06	50
CTS	-.34	.17/10	-.34	.10/20	-.19	.12/20	.13	.10/28	-.19	78
DLM	.20	.17/05	.02	.12/16	.36	.08/17	.11	.13/18	.17	56
EPN	-.08	.11/10	.21	.17/20	.18	.12/19	.21	.19/20	.13	69
EPR	.45	.17/10	.02	.17/23	.29	.16/20	.13	.15/34	.22	87
GLR	-.22	.14/06	.00	.10/18	-.31	.08/19	-.27	.11/26	-.20	69
GMN	.16	.11/02	-.05	.15/06	-.13	.10/06	.21	.12/17	.05	31
GMR	.09	.13/05	.08	.05/21	-.18	.09/13	-.11	.11/27	-.03	66
JON	.26	.19/09	-.16	.14/18	.08	.12/20	-.01	.16/19	.04	66
KRNA	-.14	.11/08	.00	.15/14	-.01	.13/18	.09	.18/19	-.01	59
LOP	-.11	.28/09	.20	.08/24	.14	.08/24	-.21	.15/26	.01	83
LSM	-.18	.27/07	.15	.10/17	.22	.06/12	-.05	.12/15	.03	51
MCX			.08	/01	.14	/01	-.19	.10/02	.01	4
MCY	.26	.09/07	.00	.11/19	.11	.09/18	-.17	.17/23	.05	67
MGM	-.06	.18/07	-.28	.14/16	-.29	.10/13	.11	.11/21	-.13	57
MTI	.17	.24/06	.04	.10/16	-.08	.10/19	.03	.20/20	.04	61
MZP	-.23	.07/05	-.33	.16/13	-.23	.14/13	-.05	.06/16	-.21	47
NMN	-.54	.08/04	-.12	.08/16	-.24	.10/16	.04	.16/22	-.22	58
NPN	.32	.24/06	.09	.11/15	.34	.10/20	.18	.10/21	.23	62
PRN	.43	.19/10	.04	.14/20	.32	.09/18	.13	.11/29	.23	77
QCS	.02	.15/05	.12	.10/21	-.23	.10/18	.06	.09/17	-.01	61
RVE	.07	.13/04	.01	.09/06	-.06	.09/04	-.06	.07/03	-.01	17
SDH	.09	.05/07	-.07	.08/17	-.02	.08/20	-.13	.11/19	-.03	63
SGV	-.23	.25/10	.03	.10/21	-.13	.15/19	.09	.20/27	-.08	77
SHRG	.27	.10/07	-.05	.09/20	.26	.13/18	.18	.18/17	.17	62
SPRG	.32	.08/09	.03	.14/20	.18	.08/20	-.32	.16/23	.05	72
SRG	.13	.14/04	.14	.12/19	.18	.10/18	.18	.16/27	.16	68
SSP	-.23	.20/08	.12	.08/20	.05	.08/19	-.14	.19/19	-.05	66
SVP	-.08	.20/03	.01	.17/13	.12	.12/11	.19	.13/10	.06	37
TNP	-.19	.10/05	-.03	.19/13	.02	.16/09	.10	.15/16	-.03	43
TPU	.09	.13/03	.03	.06/14	-.33	.10/17	-.13	.08/19	-.09	53
WRN	-.06	/01	.06	.11/06	-.17	.05/05	.04	.11/08	-.03	20

TABLE 8

Model nov9b with various damping parameters

Name	Velocity perturbations			Diagonal Elements			Standard Errors			Number
Damping:	.0030	.0020	.0050	.0030	.0020	.0050	.0030	.0020	.0050	
AMR	0.45	0.35	0.48	.80	.84	.75	.56	.62	.50	72
APK	3.45	4.15	2.67	.64	.68	.58	.62	.75	.50	60
BGB	1.83	1.68	2.00	.86	.89	.83	.46	.51	.42	84
BLT	0.50	0.38	0.62	.66	.70	.61	.59	.73	.46	81
BMT	2.20	2.36	1.99	.71	.76	.64	.66	.76	.54	55
BRO	-1.29	-1.34	-1.25	.77	.81	.71	.62	.70	.52	69
CDH1	-1.52	-1.73	-1.24	.72	.78	.63	.74	.82	.64	14
CPX	0.65	0.72	0.55	.84	.87	.79	.54	.58	.49	50
CTS	2.47	2.46	2.40	.69	.73	.62	.64	.73	.52	78
DLM	1.36	1.56	1.12	.61	.66	.55	.61	.73	.48	56
EPN	-7.00	-7.38	-6.46	.81	.84	.75	.57	.64	.50	69
EPR	-4.50	-4.86	-3.96	.63	.67	.57	.61	.73	.48	87
FMT	-3.00	-3.30	-2.65	.78	.82	.71	.62	.69	.53	55
GLR	0.93	0.76	1.11	.80	.84	.75	.57	.64	.50	69
GMN	-0.66	-0.54	-0.75	.78	.82	.71	.63	.69	.56	31
GMR	-2.25	-2.40	-2.04	.78	.82	.72	.59	.66	.51	66
GVN	-5.85	-6.21	-5.33	.77	.80	.72	.56	.63	.48	63
GWV	1.00	0.64	1.30	.65	.70	.58	.65	.77	.51	56
JON	2.17	2.48	1.76	.82	.86	.77	.56	.61	.50	66
KRN	----	----	----	---	---	---	---	---	---	0
KRNA	-2.38	-2.52	-2.15	.72	.76	.66	.61	.69	.52	59
LCH	5.14	5.75	4.37	.72	.76	.66	.60	.69	.49	62
LOP	-1.19	-1.27	-1.06	.86	.89	.82	.47	.51	.43	83
LSM	-4.39	-4.49	-4.18	.84	.87	.79	.54	.58	.49	51
MCA	0.51	0.19	0.75	.63	.68	.57	.63	.75	.50	66
MCX	0.77	1.07	0.48	.48	.57	.36	.88	1.05	.67	4
MCY	3.27	3.70	2.74	.80	.83	.74	.57	.63	.49	67
MGM	3.55	3.85	3.15	.72	.77	.66	.61	.70	.51	57
MTI	0.01	0.13	-0.06	.78	.81	.72	.58	.64	.50	61
MZP	5.39	5.58	5.05	.65	.69	.59	.60	.71	.49	47
NEL	----	----	----	---	---	---	---	---	---	0
NMN	1.18	1.30	1.02	.80	.84	.75	.59	.64	.52	58
NPN	-2.67	-2.60	-2.62	.78	.81	.73	.53	.58	.47	62
NOP	2.10	2.29	1.81	.67	.72	.60	.65	.76	.52	78
PGE	-1.74	-2.27	-1.22	.59	.63	.53	.62	.75	.49	57
PPK	-0.47	-0.20	-0.80	.65	.70	.59	.64	.77	.50	68
PRN	-2.51	-2.72	-2.13	.74	.78	.68	.61	.68	.51	77
QCS	-2.78	-2.92	-2.52	.67	.72	.60	.66	.78	.52	61
QSM	-0.98	-1.48	-0.45	.45	.48	.41	.50	.60	.40	57
RVE	1.50	1.69	1.29	.58	.63	.50	.67	.78	.55	17
SDH	1.63	1.73	1.50	.81	.85	.75	.59	.64	.51	63
SGV	-1.86	-1.97	-1.68	.71	.76	.65	.62	.73	.50	77
SHRG	2.13	2.77	1.49	.40	.44	.36	.52	.65	.39	62
SPRG	3.43	3.94	2.79	.78	.82	.73	.57	.65	.49	72
SRG	-0.08	0.36	-0.53	.66	.71	.60	.63	.74	.51	68
SSP	0.45	0.34	0.60	.86	.89	.82	.49	.53	.45	66
SVP	1.40	1.04	1.58	.59	.63	.54	.57	.69	.46	37

TABLE 8 (continued)

Model nov9b with various damping parameters

Name	Velocity perturbations			Diagonal Elements			Standard Errors			Number
Damping:	.0030	.0020	.0050	.0030	.0020	.0050	.0030	.0020	.0050	
TMO	-1.58	-2.00	-1.10	.72	.77	.66	.62	.71	.51	53
TNP	-3.41	-3.97	-2.69	.46	.50	.42	.52	.63	.42	43
TPK	----	----	----	---	---	---	---	---	---	0
TPU	1.66	1.70	1.63	.78	.82	.71	.60	.67	.52	53
WRN	1.54	1.85	1.15	.64	.70	.55	.75	.86	.61	20

TABLE 9

Model nov9b

Damping: 0.0030 $s^2/\%^2$
Observations: 2887
Block size: 35 x 35 km
Data varience: 0.0561
Variance improvement: 82.1%

Top layer modeled as station corrections
Layer offset: none
Blocks modeled: 345
Residual varience: 0.0100

Velocity (km/s)	Thickness (km)	# of Blocks
6.0	15	8 x 8
6.7	16	8 x 9
7.8	50	9 x 10
8.3	50	9 x 10
8.5	100	11 x 10

Model nov9f

Damping: 0.0030 $s^2/\%^2$
Observations: 2887
Block size: 35 x 35 km
Data varience: 0.0561
Variance improvement: 80.6%

Top layer modeled as blocks
Layer offset: none
Blocks modeled: 337
Residual varience: 0.0109

Velocity (km/s)	Thickness (km)	# of Blocks
6.0	15	8 x 8
6.7	16	8 x 9
7.8	50	9 x 10
8.3	50	9 x 10
8.5	100	11 x 10

Model nov9e

Damping: 0.0030 $s^2/\%^2$
Observations: 2887
Block size: 35 x 35 km
Data varience: 0.0561
Variance improvement: 80.7%

Top layer modeled as station corrections
(Deeper) Layer offset: 20 km northwest
Blocks modeled: 327
Residual varience: 0.0108

Velocity (km/s)	Thickness (km)	# of Blocks
6.0	15	8 x 8
6.7	16	9 x 9
7.8	50	9 x 10
8.3	50	9 x 10
8.5	100	11 x 10

Model nov9bb

Damping = 0.0030 $s^2/\%^2$
Observations: 2887
Block size: 20 x 20 km
Data varience: 0.0561
Variance improvement: 75.5%

Top layer modeled as station corrections
Layer offset: none
Blocks modeled: 388
Residual varience: 0.0138

Velocity (km/s)	Thickness (km)	# of Blocks
6.0	15	8 x 8
6.7	16	8 x 9
7.8	50	9 x 10
8.3	50	9 x 10
8.5	100	11 x 10

TABLE 10

Model nts9h

Damping: 0.0030 $s^2/\%^2$
Observations: 634
Block size: 20 x 20 km
Data varience: 0.0459
Variance improvement: 86.6%

Top layer modeled as station corrections
Layer offset: 10 km northwest
Blocks modeled: 180
Residual varience: 0.0061

Velocity (km/s)	Thickness (km)	# of Blocks
6.0	15	4 x 4
6.7	16	6 x 8
7.8	50	9 x 10
8.3	50	9 x 10
8.5	100	11 x 11

Model nts9b

Damping: 0.0030 $s^2/\%^2$
Observations: 634
Block size: 20 x 20 km
Data varience: 0.0459
Variance improvement: 87.4%

Top layer modeled as station corrections
Layer offset: none
Blocks modeled: 174
Residual varience: 0.0058

Velocity (km/s)	Thickness (km)	# of Blocks
6.0	15	4 x 4
6.7	16	6 x 8
7.8	50	9 x 10
8.3	50	9 x 10
8.5	100	11 x 11

Model nts9g

Damping: 0.0030 $s^2/\%^2$
Observations: 634
Block size: 20 x 20 km
Data varience: 0.0459
Variance improvement: 87.2%

Top layer modeled as blocks
Layer offset: none
Blocks modeled: 179
Residual varience: 0.0059

Velocity (km/s)	Thickness (km)	# of Blocks
6.0	15	8 x 8
6.7	16	6 x 8
7.8	50	9 x 10
8.3	50	9 x 10
8.5	100	11 x 11

Model nts9bb

Damping: 0.0030 $s^2/\%^2$
Observations: 634
Block size: 35 x 35 km
Data varience: 0.0459
Variance improvement: 83.8%

Top layer modeled as station corrections
Layer offset: none
Blocks modeled: 96
Residual varience: 0.0074

Velocity (km/s)	Thickness (km)	# of Blocks
6.0	15	4 x 4
6.7	16	6 x 8
7.8	50	9 x 10
8.3	50	9 x 10
8.5	100	11 x 11

TABLE 11

Station name	Model nov9b (upper crust) Velocity (km/s)	Resol.	Standard Error	Model nov9e (upper crust) Velocity (km/s)	Resol.	Standard Error	Number of Observations
AMR	0.43	.80	.56	1.16	.63	.68	72
APK	3.40	.64	.62	4.27	.59	.51	60
BGB	1.70	.86	.46	-0.11	.86	.52	84
BLT	1.25	.69	.61	-0.54	.82	.59	81
BMT	2.01	.70	.66	1.65	.74	.62	55
BRO	-1.43	.77	.62	-0.78	.79	.60	69
CDH1	-1.51	.72	.74	0.52	.73	.78	14
CPX	0.47	.84	.54	-1.79	.84	.58	50
CTS	2.57	.69	.64	1.05	.55	.49	78
DLM	1.30	.61	.61	-1.03	.71	.62	56
EPN	-7.13	.81	.58	-9.20	.84	.54	69
EPR	-4.27	.63	.61	-3.74	.62	.58	87
FMT	-3.07	.78	.62	-1.64	.76	.64	55
GLR	0.45	.80	.57	-0.93	.83	.58	69
GMN	-0.77	.78	.63	-1.07	.61	.67	31
GMR	-2.49	.79	.59	-3.01	.76	.64	66
GVN	-5.86	.77	.56	-6.34	.77	.60	63
GWV	1.09	.65	.65	4.33	.73	.67	56
JON	2.09	.82	.56	1.16	.60	.61	66
KRN	---	---	---	---	---	---	0
KRNA	-1.97	.73	.61	-0.41	.62	.63	59
LCH	5.16	.72	.60	3.57	.77	.60	62
LOP	-1.27	.86	.47	-1.53	.88	.47	83
LSM	-4.45	.84	.54	-2.31	.84	.57	51
MCA	0.59	.63	.63	1.00	.67	.63	66
MCX	0.66	.48	.88	0.73	.47	.91	4
MCY	3.09	.80	.57	3.35	.84	.54	67
MGM	3.54	.72	.61	5.85	.78	.60	57
MTI	0.19	.78	.58	0.41	.66	.66	61
MZP	5.21	.65	.60	7.33	.70	.65	47
NEL	---	---	---	---	---	---	0
NMN	0.97	.80	.59	-0.91	.68	.66	58
NOP	2.14	.67	.65	3.20	.62	.62	78
NPN	-2.62	.78	.53	-2.97	.73	.57	62
PGE	-1.65	.59	.62	-0.43	.68	.68	57
PPK	-0.43	.65	.64	-3.78	.87	.47	68
PRN	-2.40	.74	.60	-1.06	.67	.56	77
QCS	-2.13	.67	.66	-1.10	.64	.60	61
QSM	-0.81	.45	.50	2.47	.69	.72	57
RVE	1.57	.57	.67	0.46	.56	.70	17
SDH	1.53	.81	.59	1.96	.83	.57	63
SGV	1.83	.71	.62	-2.72	.81	.54	77
SHRG	2.08	.40	.52	2.45	.51	.61	62
SPRG	3.28	.78	.57	3.94	.80	.59	72
SRG	-0.23	.66	.63	-2.55	.68	.58	68
SSP	0.38	.86	.49	-1.19	.88	.49	66
SVP	1.30	.59	.57	1.53	.80	.63	37
TMO	-1.54	.72	.62	-1.87	.70	.59	53

TABLE 11 (continued)

	Model nov9b (upper crust)			Model nov9e (upper crust)			
Station name	Velocity (km/s)	Resol.	Standard Error	Velocity (km/s)	Resol.	Standard Error	Number of Observations
TNP	-3.60	.46	.52	-1.21	.44	.58	43
TPK	---	---	---	---	---	---	0
TPU	2.16	.78	.60	1.43	.65	.64	53
WRN	1.48	.64	.75	0.48	.43	.51	20

TABLE 12

Model nts9h

Station	Velocity Perturbation	Diagonal Element	Standard Error
BGB	1.71	.74	.43
BMT	5.33	.57	.37
CDH1	-1.05	.57	.53
CPX	-0.22	.71	.44
EPN	-4.56	.66	.41
GLR	1.61	.50	.37
LOP	-1.03	.79	.37
LSM	-3.67	.64	.46
MCY	0.82	.62	.41
SPRG	0.58	.57	.41
SSP	0.58	.79	.38

Model nts9b

Station	Velocity Perturbation	Diagonal Element	Standard Error
BGB	2.08	.78	.37
BMT	3.83	.57	.37
CDH1	0.36	.60	.54
CPX	-0.59	.71	.42
EPN	-3.53	.67	.40
GLR	0.83	.61	.43
LOP	-0.77	.79	.37
LSM	-2.23	.67	.45
MCY	0.64	.69	.41
SPRG	0.20	.65	.39
SSP	-0.03	.79	.38

Model nts9bb

Station	Velocity Perturbation	Diagonal Element	Standard Error
BGB	2.35	.82	.38
BMT	5.56	.57	.52
CDH1	-0.98	.65	.63
CPX	-0.16	.75	.51
EPN	-5.06	.71	.50
GLR	1.57	.56	.57
LOP	-1.84	.82	.40
LSM	-3.38	.70	.51
MCY	0.15	.65	.51
SPRG	0.75	.68	.48
SSP	1.16	.83	.40

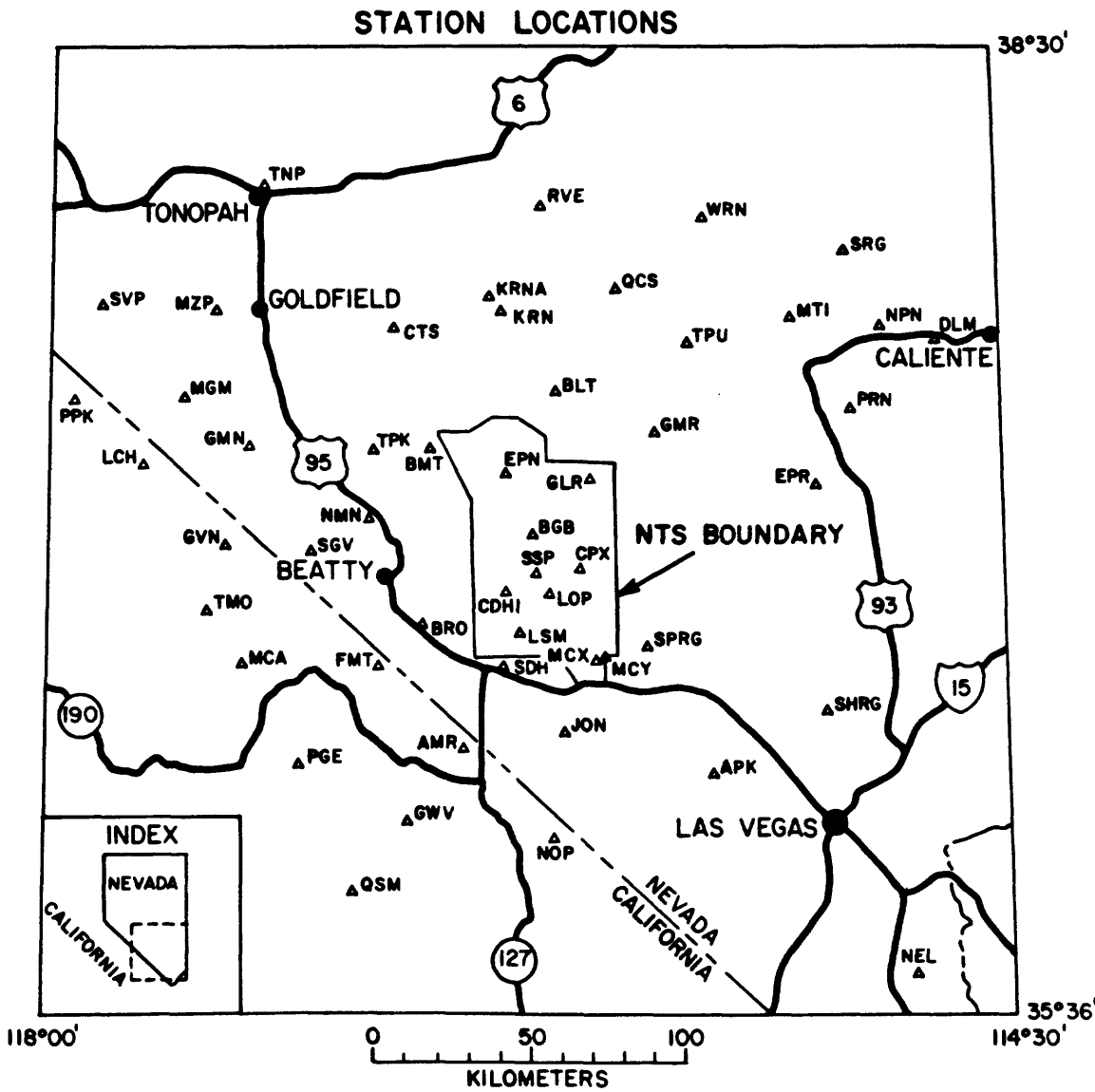

Figure 1. Southern Nevada-southeastern California seismic network of the U. S. Geological Survey. These are 1 Hz vertical-component stations. The Nevada Test Site (NTS) boundary is shown for reference.

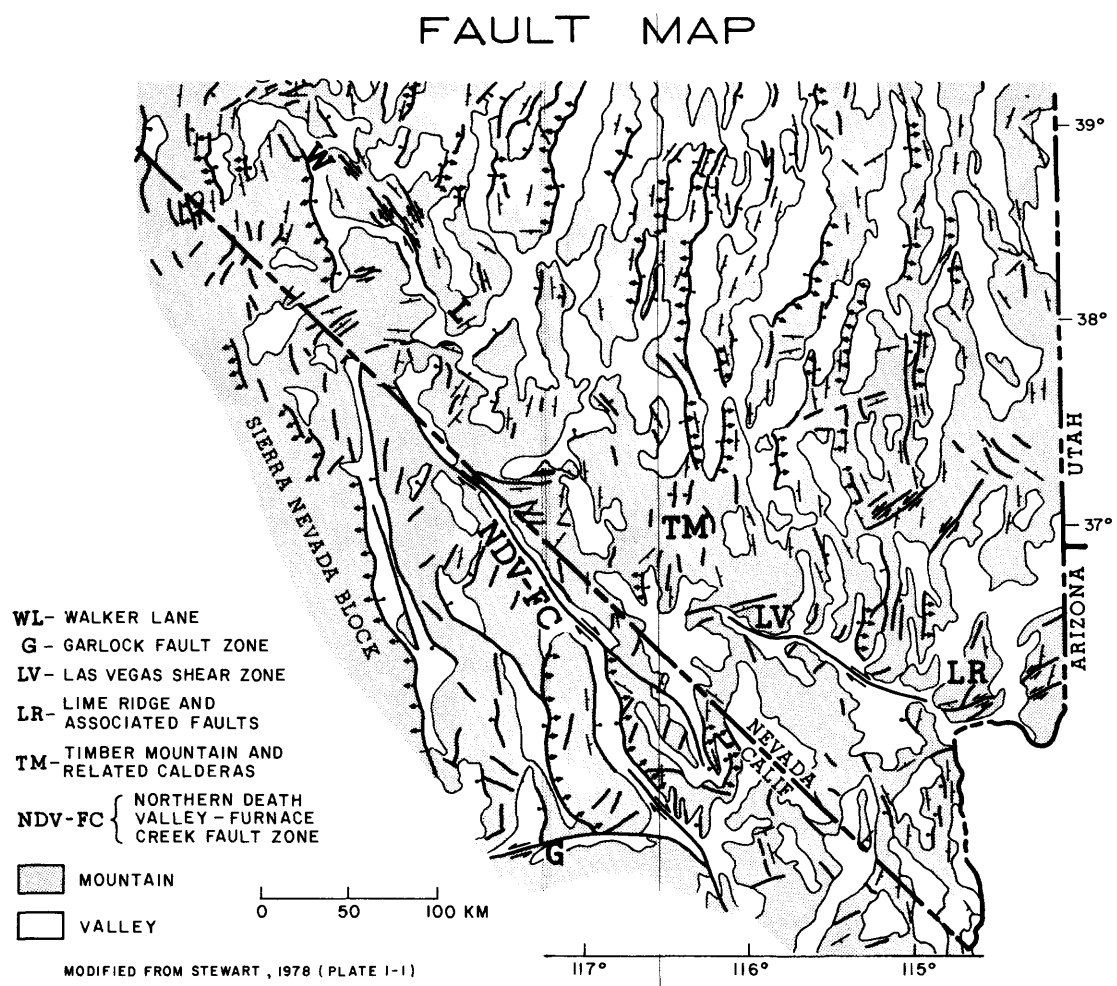

Figure 2. Fault map of the southern Nevada-southeastern California region. Major faults and shear zones are labeld; Walker Lane extends southeast across Nevada as indicated by the "W" and "L."

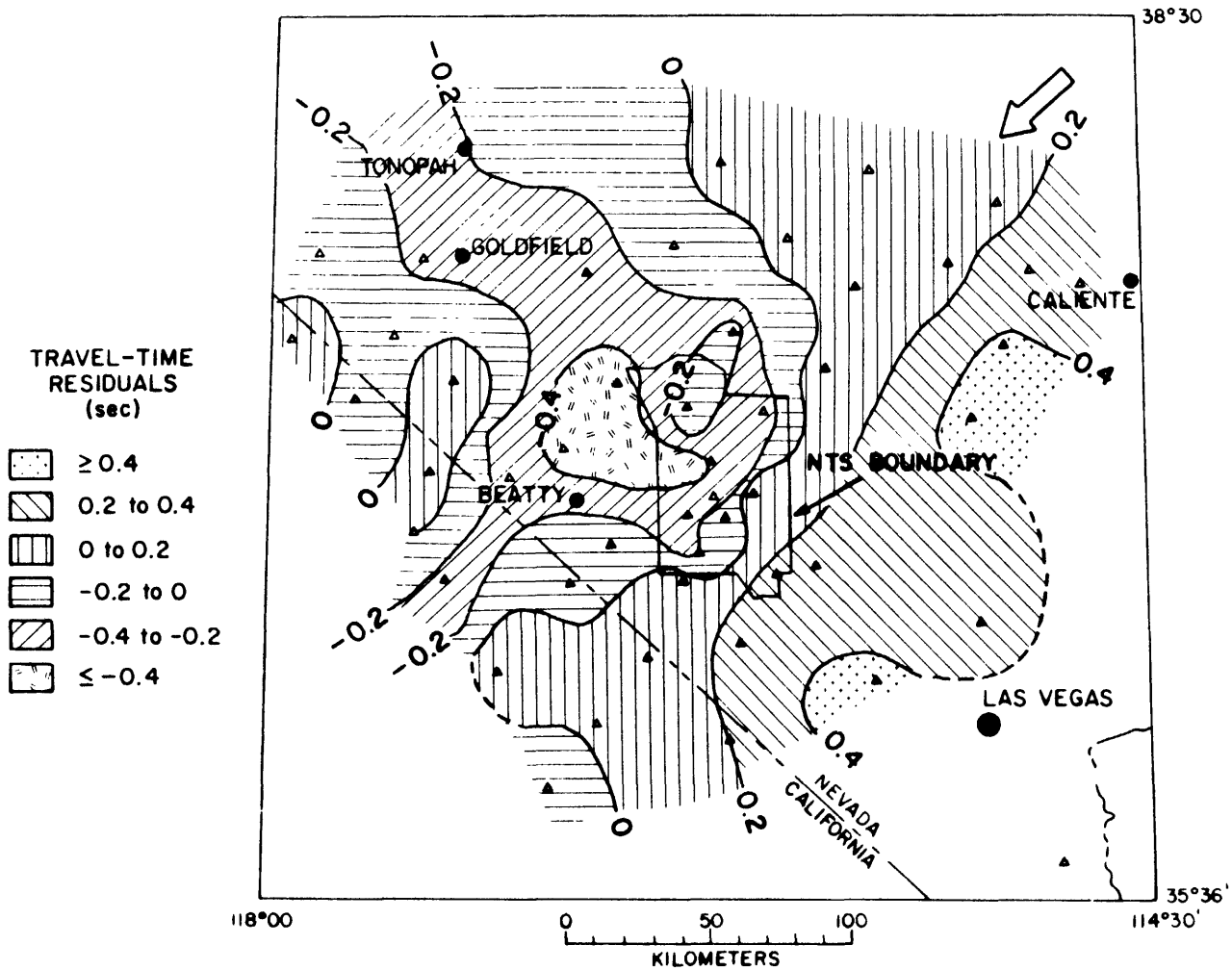

Figure 3. Average relative residuals for the whole network for events in the (a) northeast, (b) southeast, (c) southwest, (d) northwest, and (e) all quadrants. Positive values are late arrivals.

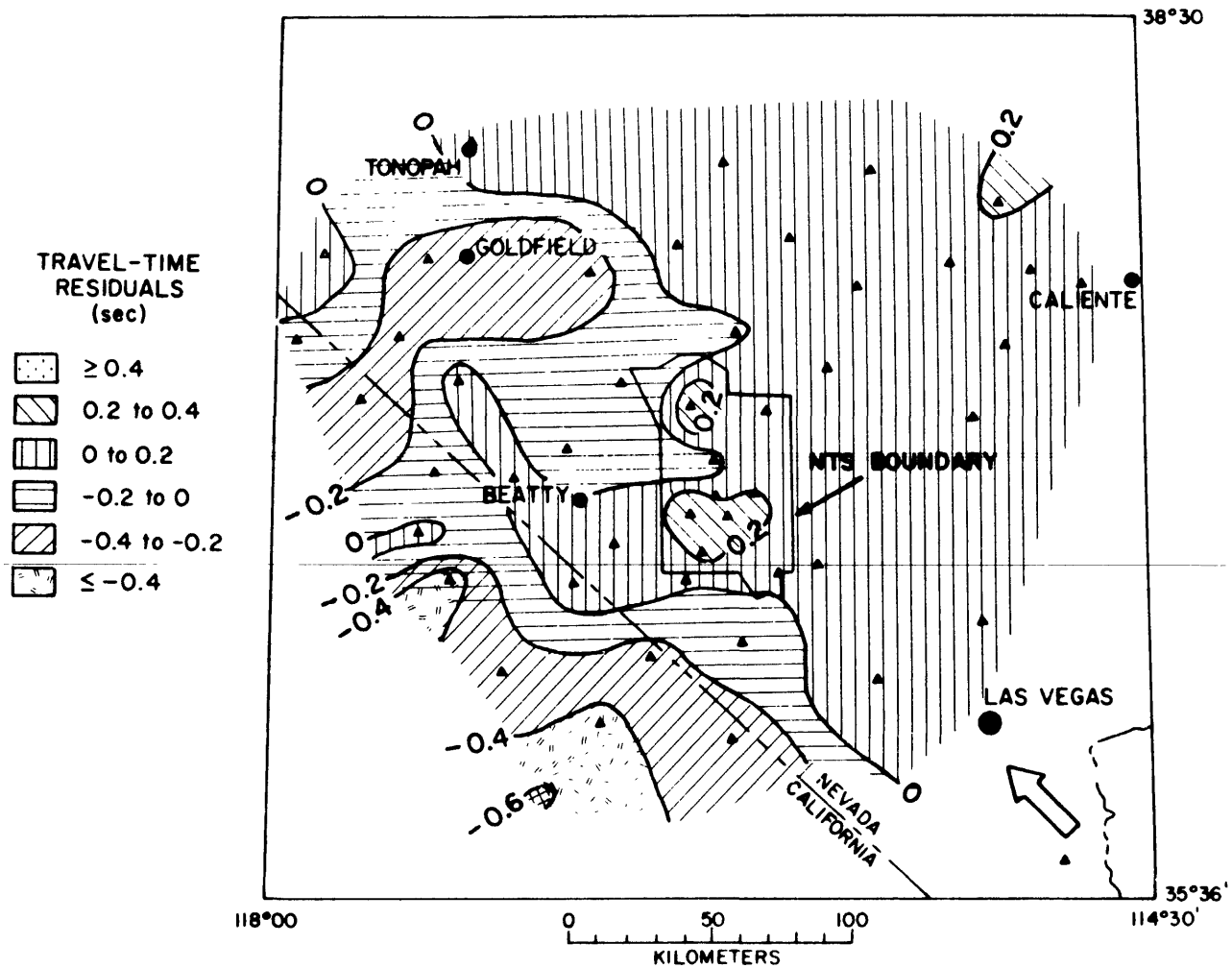
TRAVEL-TIME RESIDUALS (sec)
≥ 0.4
0.2 to 0.4
0 to 0.2
-0.2 to 0
-0.4 to -0.2
≤ -0.4
TONOPAH
GOLDFIELD
BEATTY
CALIENTE
LAS VEGAS
NTS BOUNDARY
NEVADA
CALIFORNIA
38°30
35°36'
118°00
114°30'
0
50
100
KILOMETERS

Figure 3b

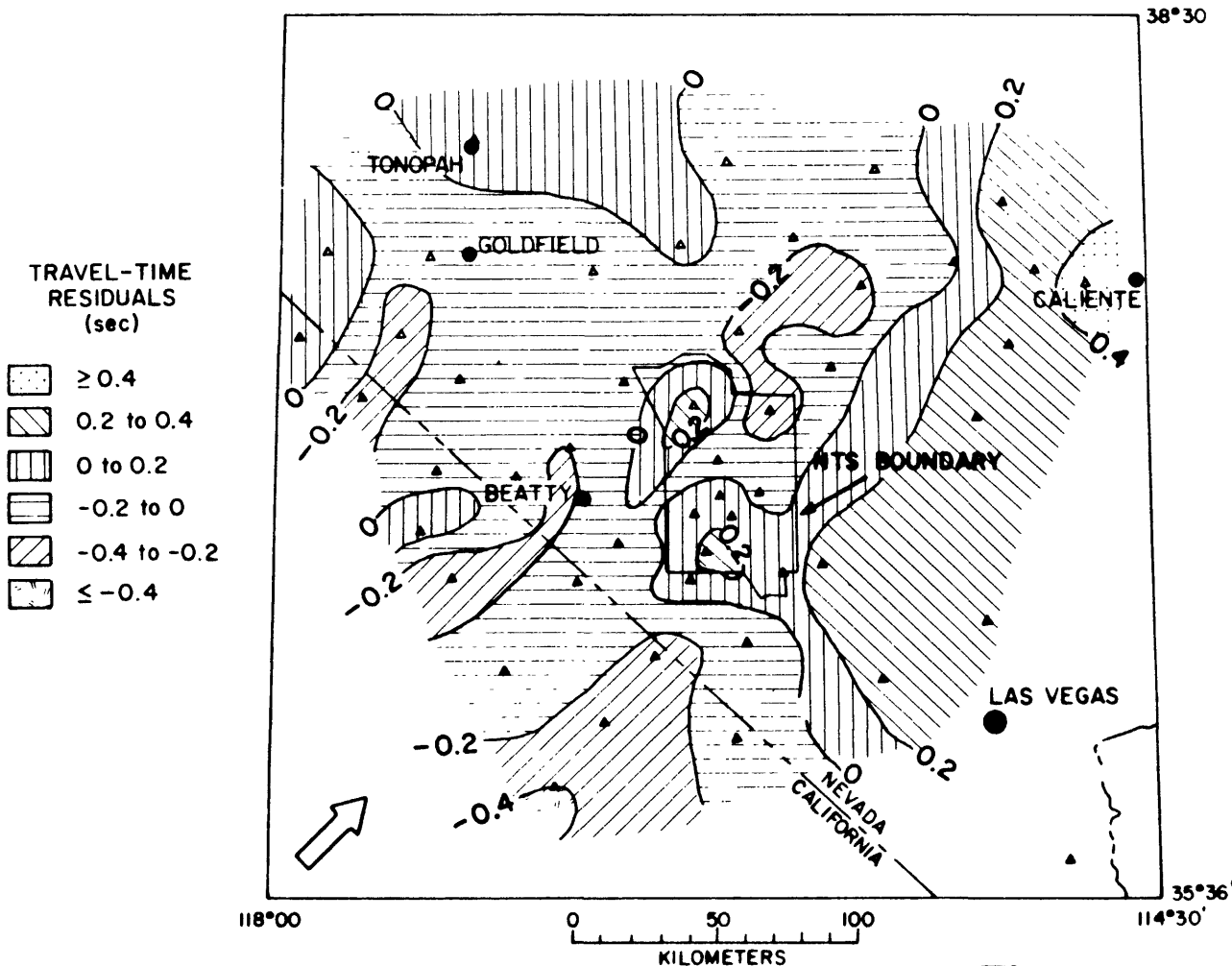
TRAVEL-TIME RESIDUALS (sec)
≥ 0.4
0.2 to 0.4
0 to 0.2
-0.2 to 0
-0.4 to -0.2
≤ -0.4
38°30
35°36'
118°00
114°30'
TONOPAH
GOLDFIELD
BEATTY
CALIENTE
LAS VEGAS
NTS BOUNDARY
NEVADA
CALIFORNIA
0
50
100
KILOMETERS

Figure 3c

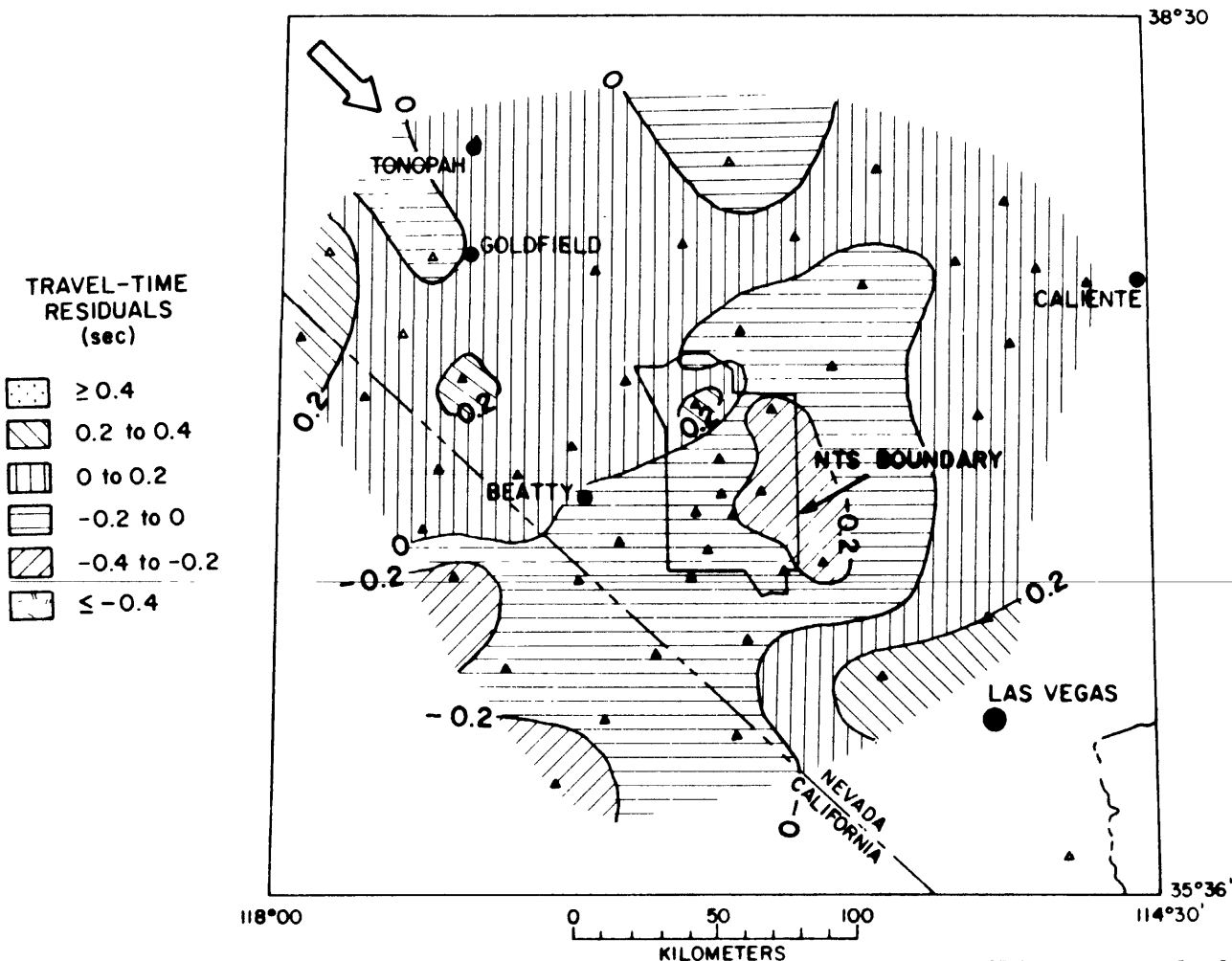
TRAVEL-TIME RESIDUALS (sec)
≥ 0.4
0.2 to 0.4
0 to 0.2
-0.2 to 0
-0.4 to -0.2
≤ -0.4
38°30
TONOPAH
GOLDFIELD
CALIENTE
BEATTY
NTS BOUNDARY
LAS VEGAS
NEVADA
CALIFORNIA
35°36'
118°00
114°30'
0
50
100
KILOMETERS

Figure 3d

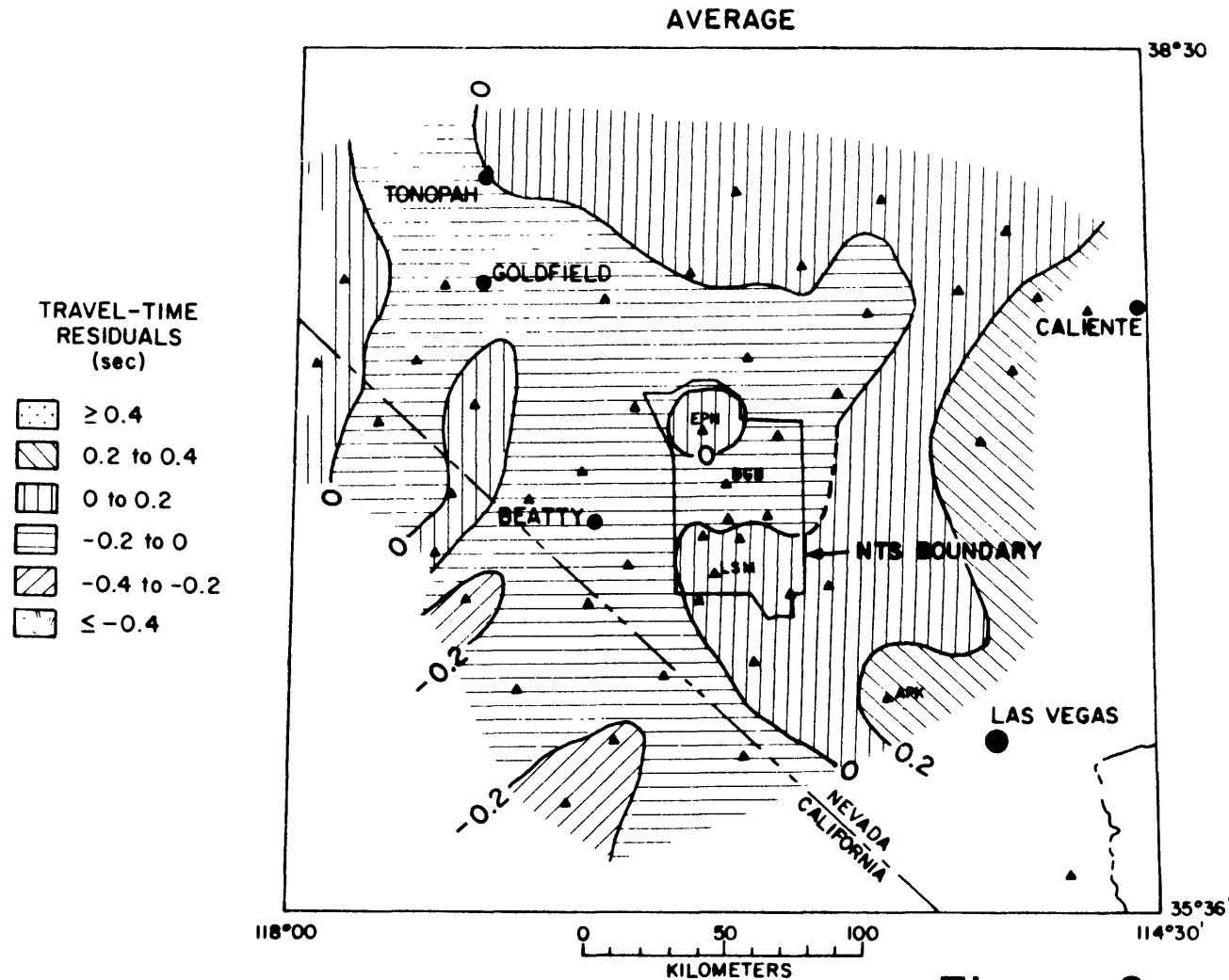
AVERAGE
TRAVEL-TIME RESIDUALS (sec)
≥ 0.4
0.2 to 0.4
0 to 0.2
-0.2 to 0
-0.4 to -0.2
≤ -0.4
38°30
TONOPAH
GOLDFIELD
CALIENTE
EPN
BEATTY
NTS BOUNDARY
LAS VEGAS
ARK
NEVADA
CALIFORNIA
35°36'
118°00
114°30'
0
50
100
KILOMETERS

Figure 3e

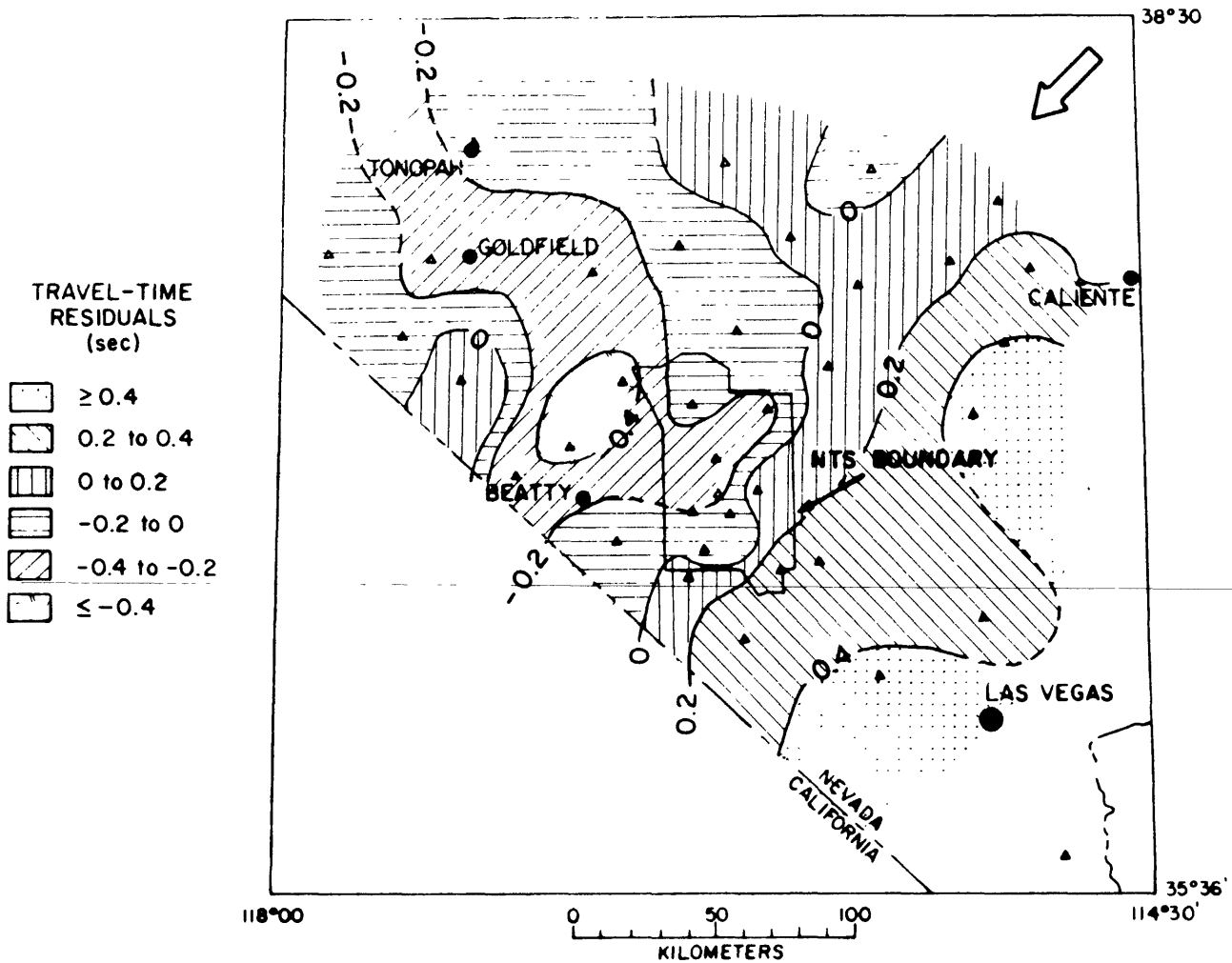

Figure 4. Same as Figure 3 but only for stations northeast of the northern Death Valley-Furnace Creek fault zone.

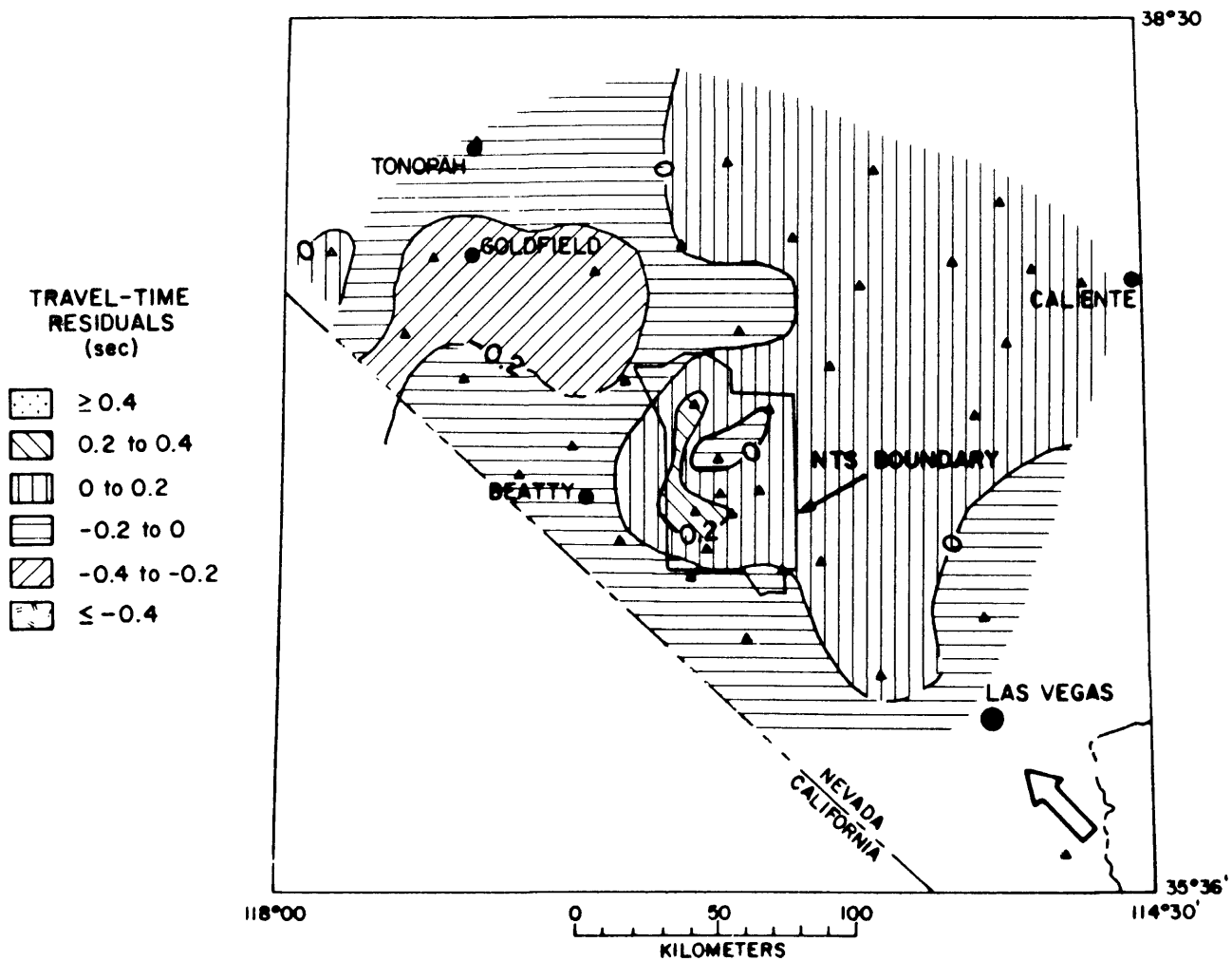
TRAVEL-TIME RESIDUALS (sec)
≥ 0.4
0.2 to 0.4
0 to 0.2
-0.2 to 0
-0.4 to -0.2
≤ -0.4
38°30
TONOPAH
GOLDFIELD
CALIENTE
BEATTY
NTS BOUNDARY
LAS VEGAS
NEVADA
CALIFORNIA
35°36'
118°00
114°30'
0
50
100
KILOMETERS

Figure 4b

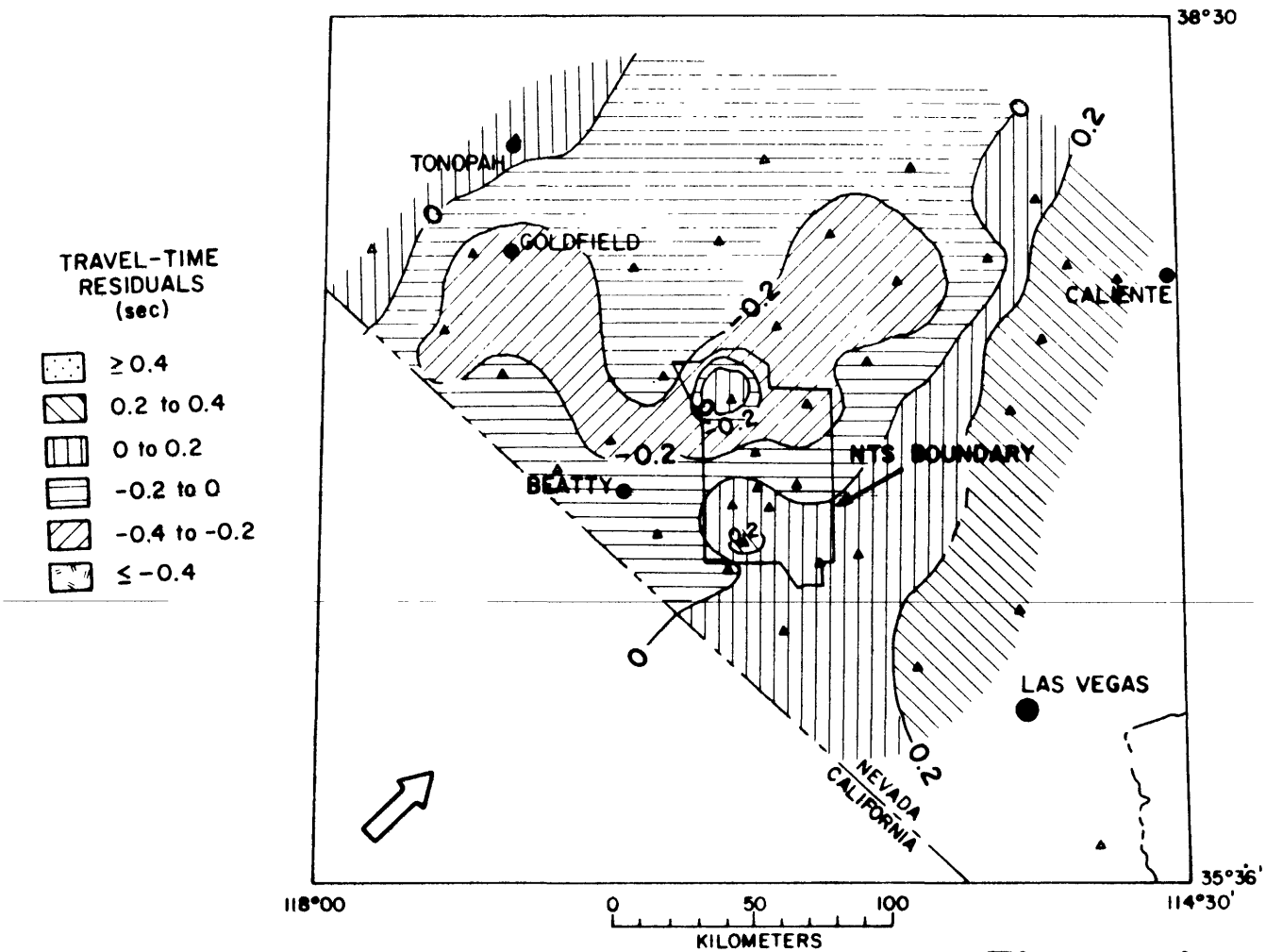
TRAVEL-TIME RESIDUALS (sec)
≥ 0.4
0.2 to 0.4
0 to 0.2
-0.2 to 0
-0.4 to -0.2
≤ -0.4
38°30
TONOPAH
GOLDFIELD
CALIENTE
BEATTY
NTS BOUNDARY
LAS VEGAS
NEVADA
CALIFORNIA
0
0.2
-0.2
-0.4
35°36'
118°00
114°30'
0
50
100
KILOMETERS

Figure 4c

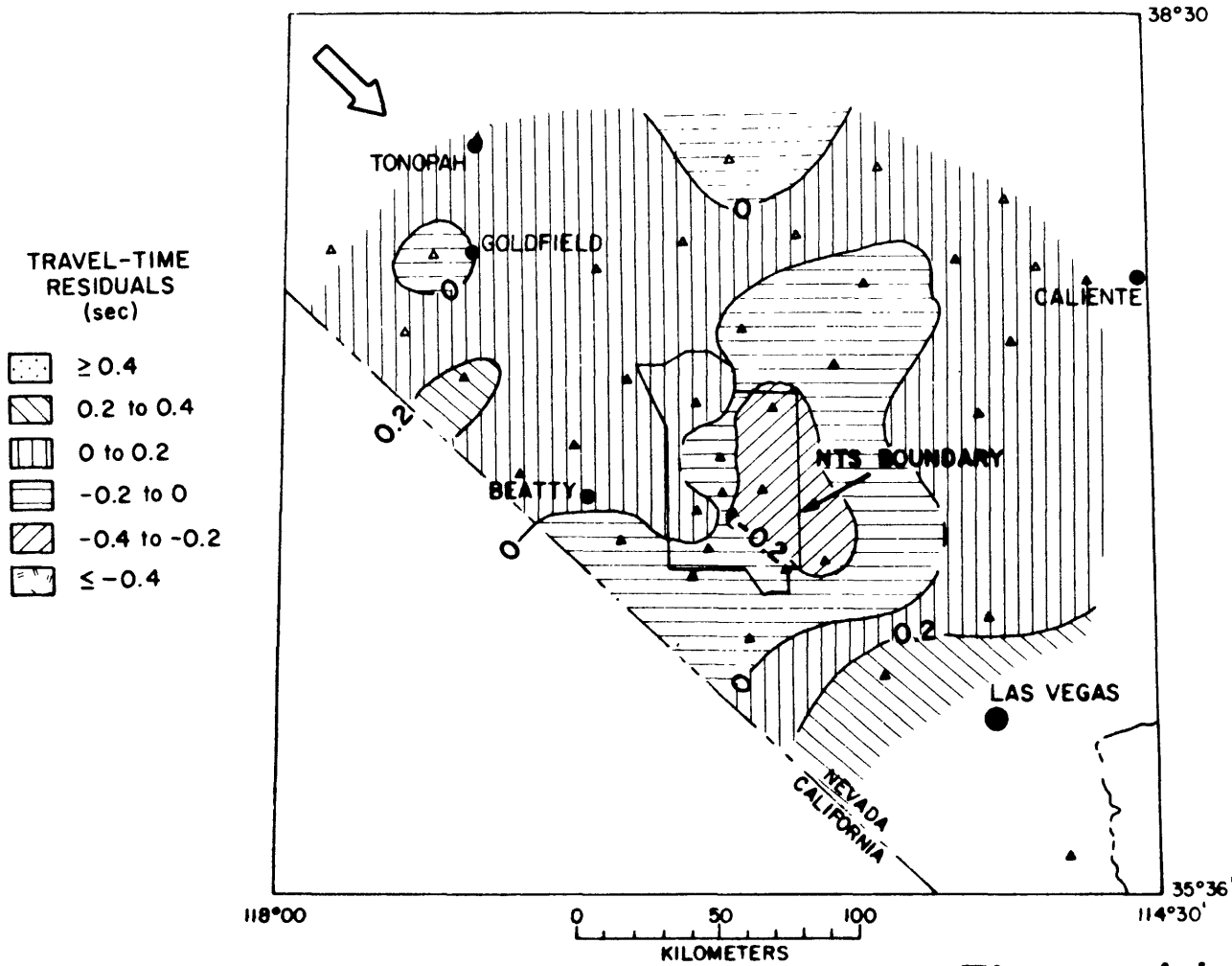
TRAVEL-TIME RESIDUALS (sec)
≥ 0.4
0.2 to 0.4
0 to 0.2
-0.2 to 0
-0.4 to -0.2
≤ -0.4
TONOPAH
GOLDFIELD
CALIENTE
BEATTY
NTS BOUNDARY
LAS VEGAS
NEVADA
CALIFORNIA
0
0.2
-0.2
38°30
35°36'
118°00
114°30'
0
50
100
KILOMETERS

Figure 4d

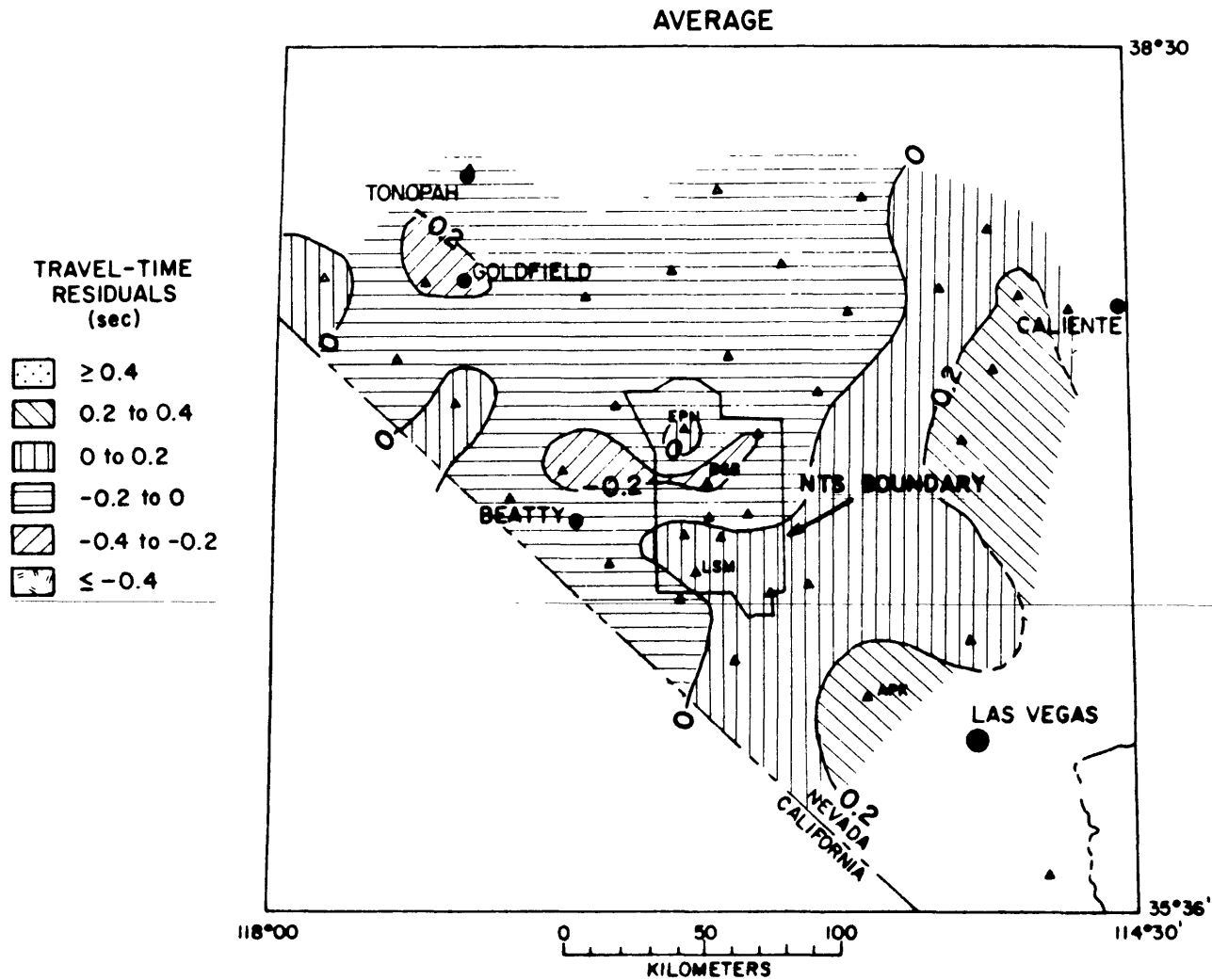
AVERAGE
TRAVEL-TIME RESIDUALS (sec)
≥ 0.4
0.2 to 0.4
0 to 0.2
-0.2 to 0
-0.4 to -0.2
≤ -0.4
38°30
TONOPAH
GOLDFIELD
CALIENTE
EPN
NTS BOUNDARY
BEATTY
LSM
LAS VEGAS
NEVADA
CALIFORNIA
35°36'
118°00
114°30'
0
50
100
KILOMETERS

Figure 4e

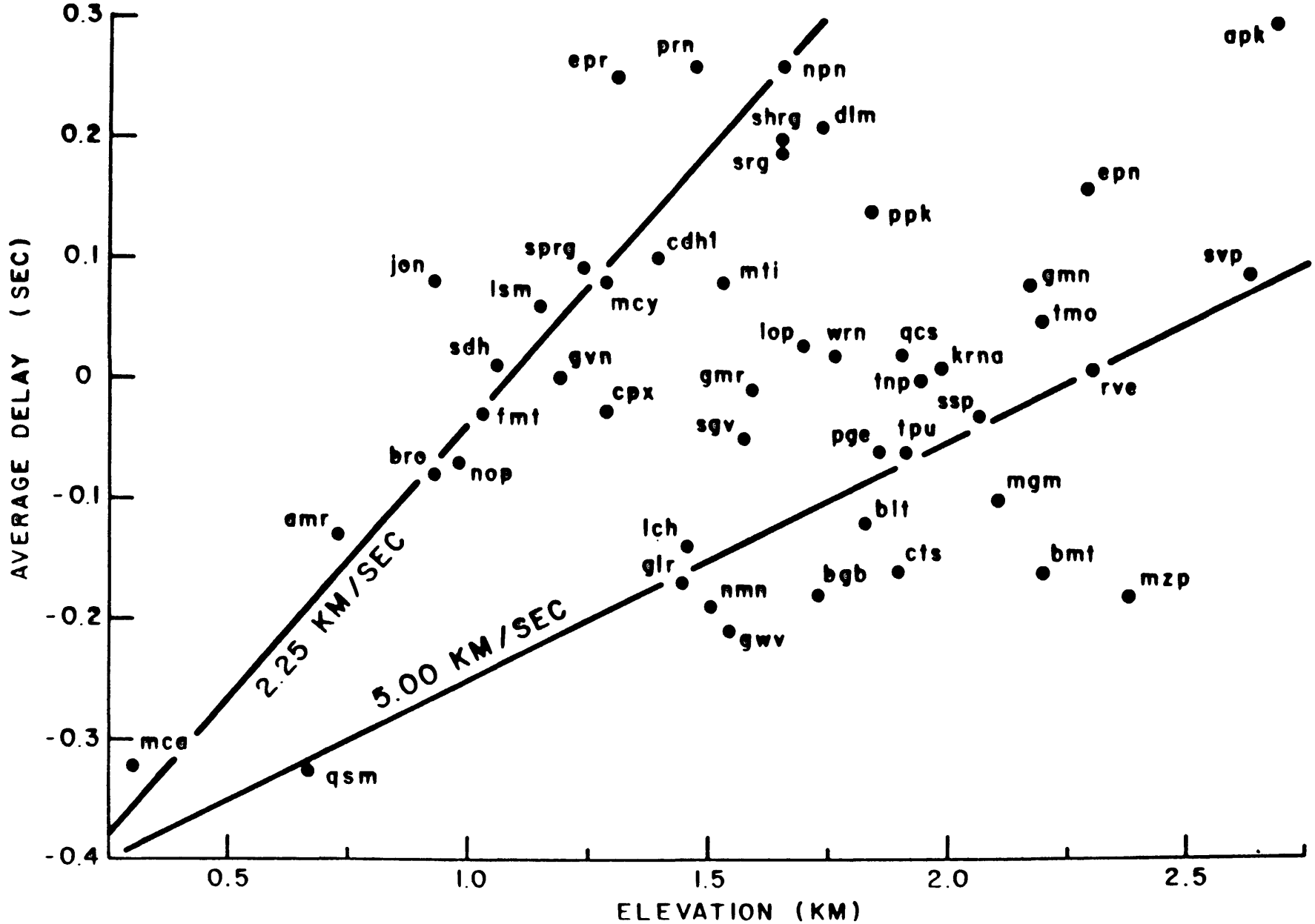

Figure 5. Station elevation versus mean relative residuals.

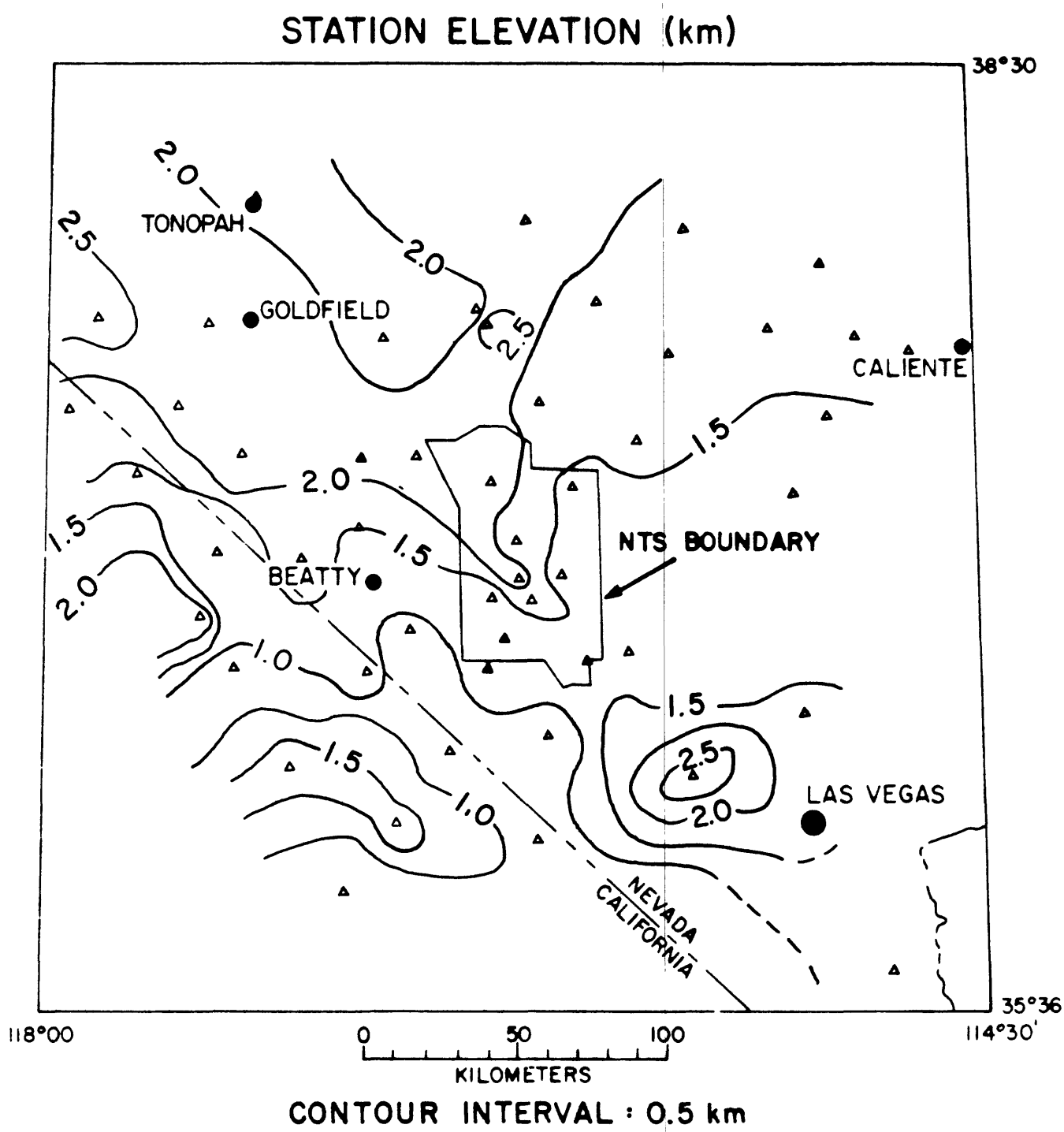

Figure 6. Station elevations (not topography). Contour interval is 0.5 km.

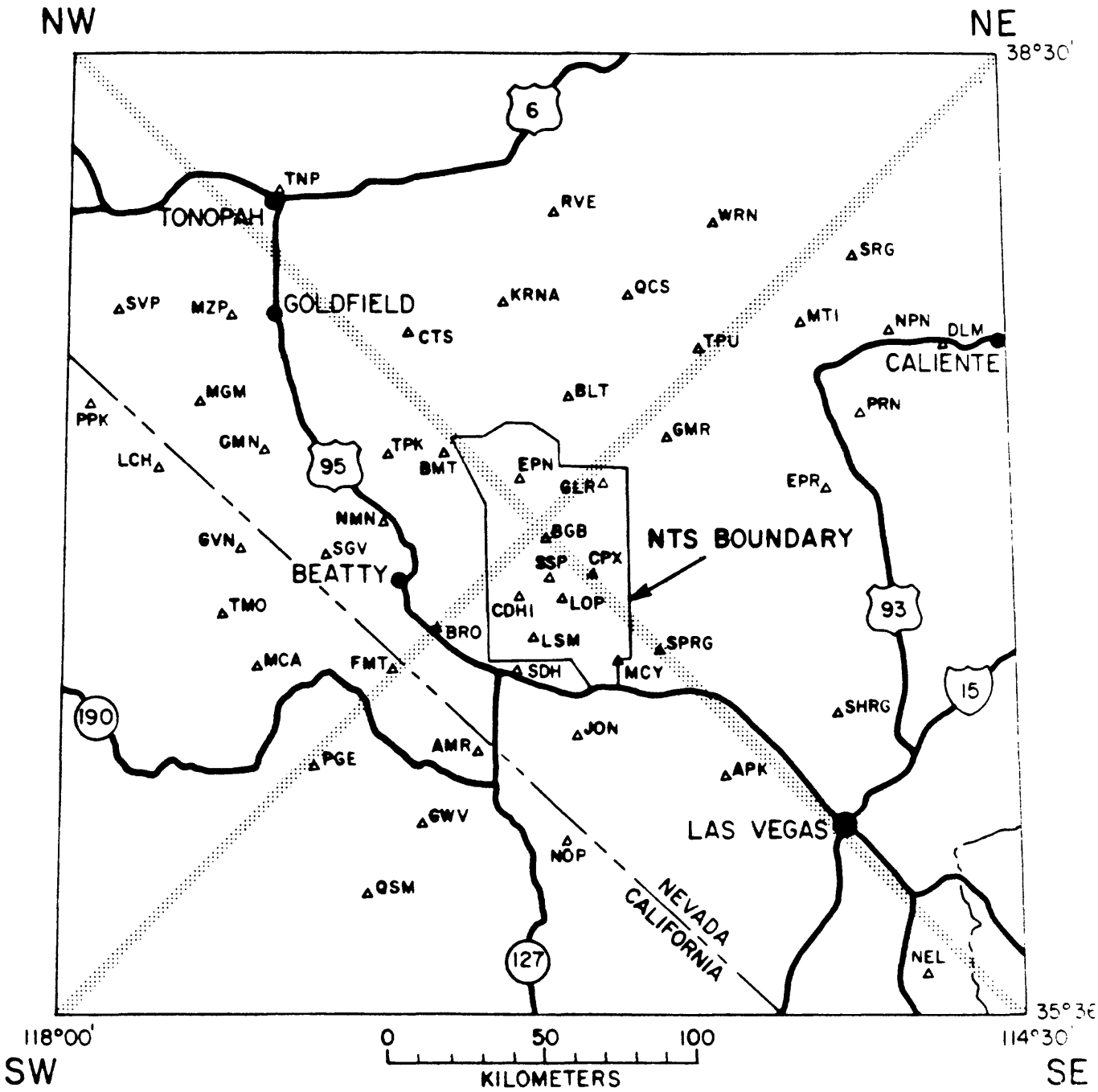

Figure 7. (a) Map of the stations showing the strike and general path of the two narrow profiles of stations shown in part "b". (b) Average relative residuals along those profiles. For the northwest-striking profile, averages for the northwest quadrant are shown with a solid line and for the southeast quadrant with a dashed line. For the northeast striking line, data for the southwest quadrant are shown as a solid line and for the northeast quadrant as a dashed line.

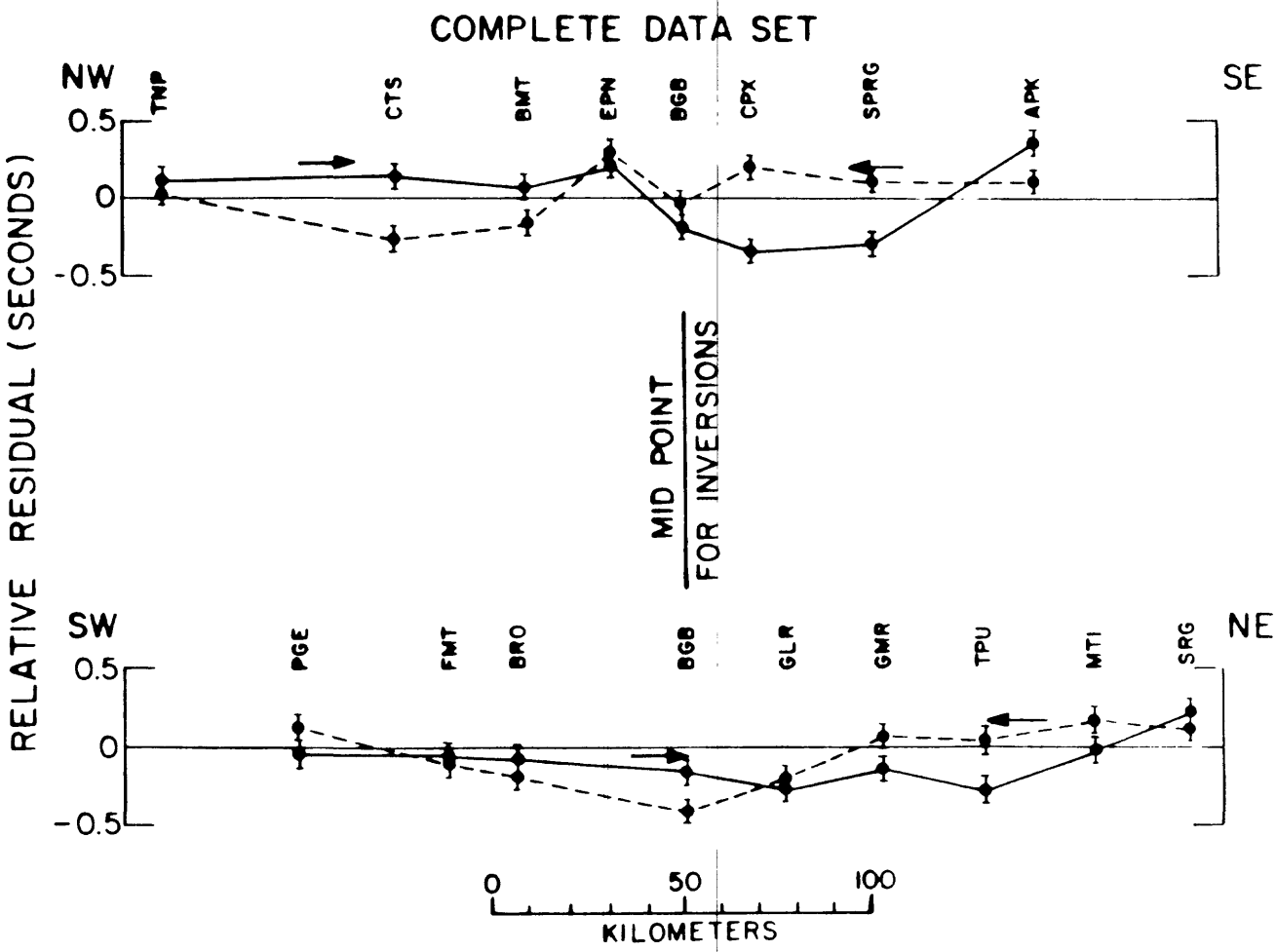
COMPLETE DATA SET
NW
SE
SW
NE
TNP
CTS
BMT
EPN
BGB
CPX
SPRG
APK
PGE
FMT
BRO
BGB
GLR
GMR
TPU
MTI
SRG
0.5
0
-0.5
RELATIVE RESIDUAL (SECONDS)
MID POINT
FOR INVERSIONS
0
50
100
KILOMETERS

Figure 7b

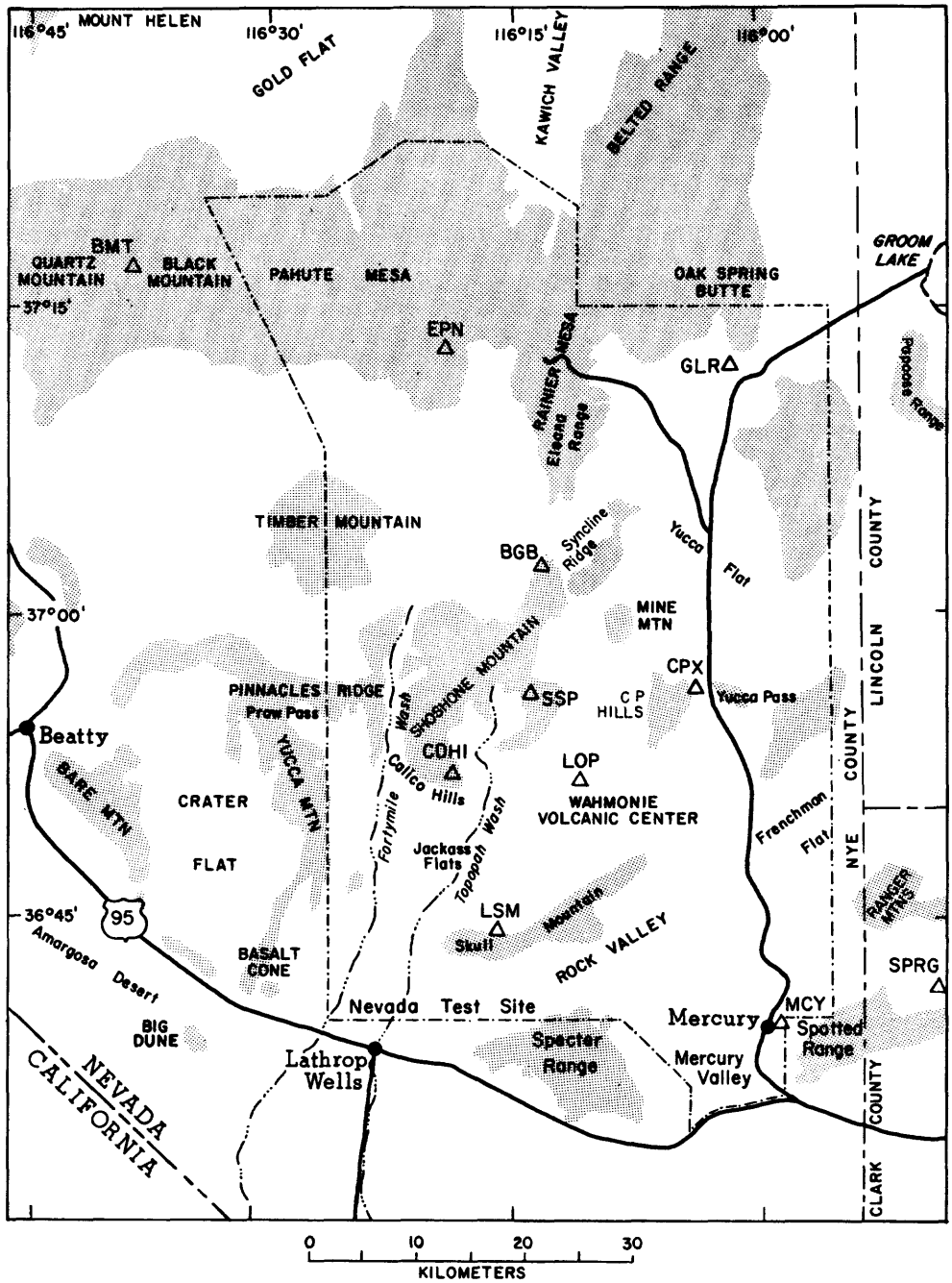

MODIFIED FROM HOOVER AND OTHERS (1981)

Figure 8. Map of the Nevada Test Site (NTS) showing stations used in the detailed inversions (model nts9b) and names of physiographic features.

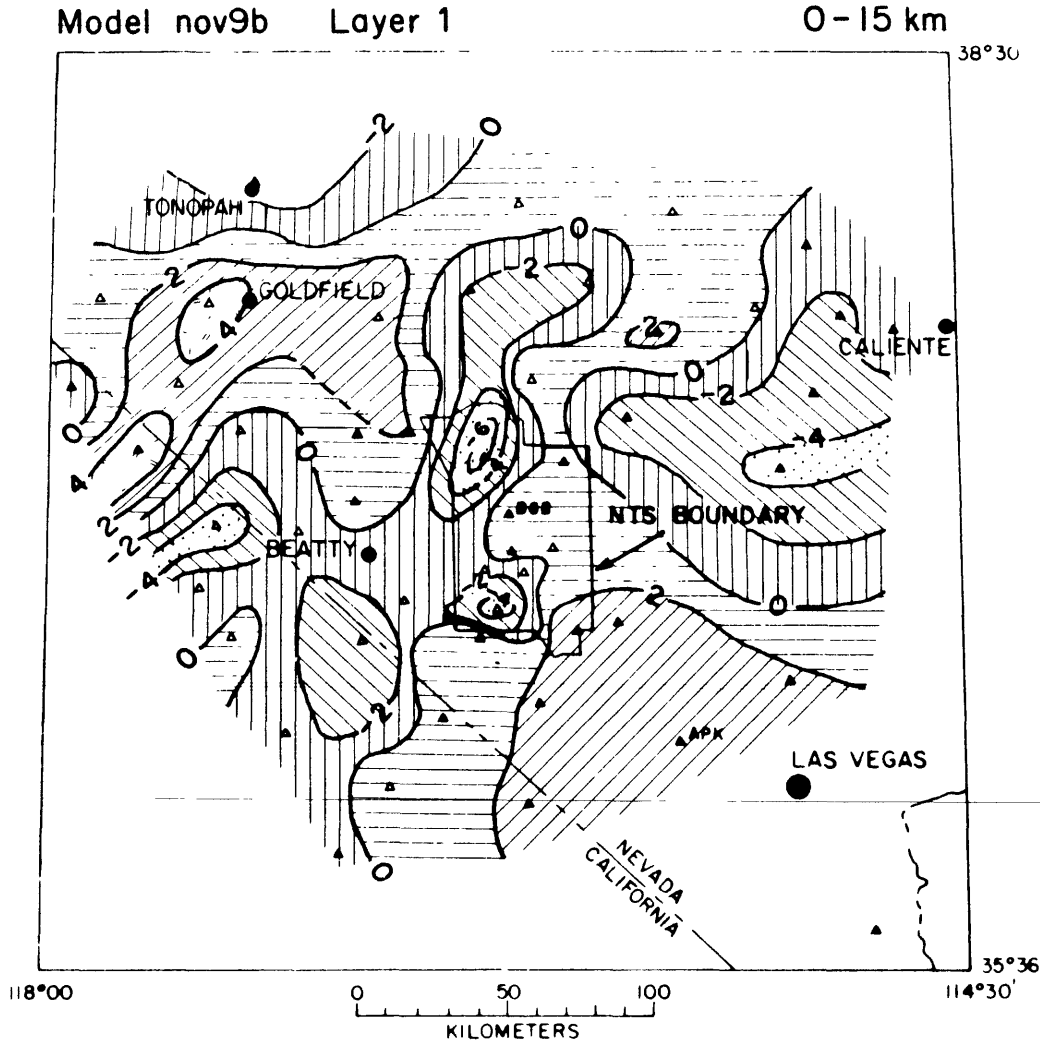

Figure 9. The upper layer of model nov9b (for the case modeling the upper layer as "station corrections"). Positive velocity perturbations (%) are relative high velocities. Zero perturbation is the mean layer velocity. Other layers are shown in Figure 10.

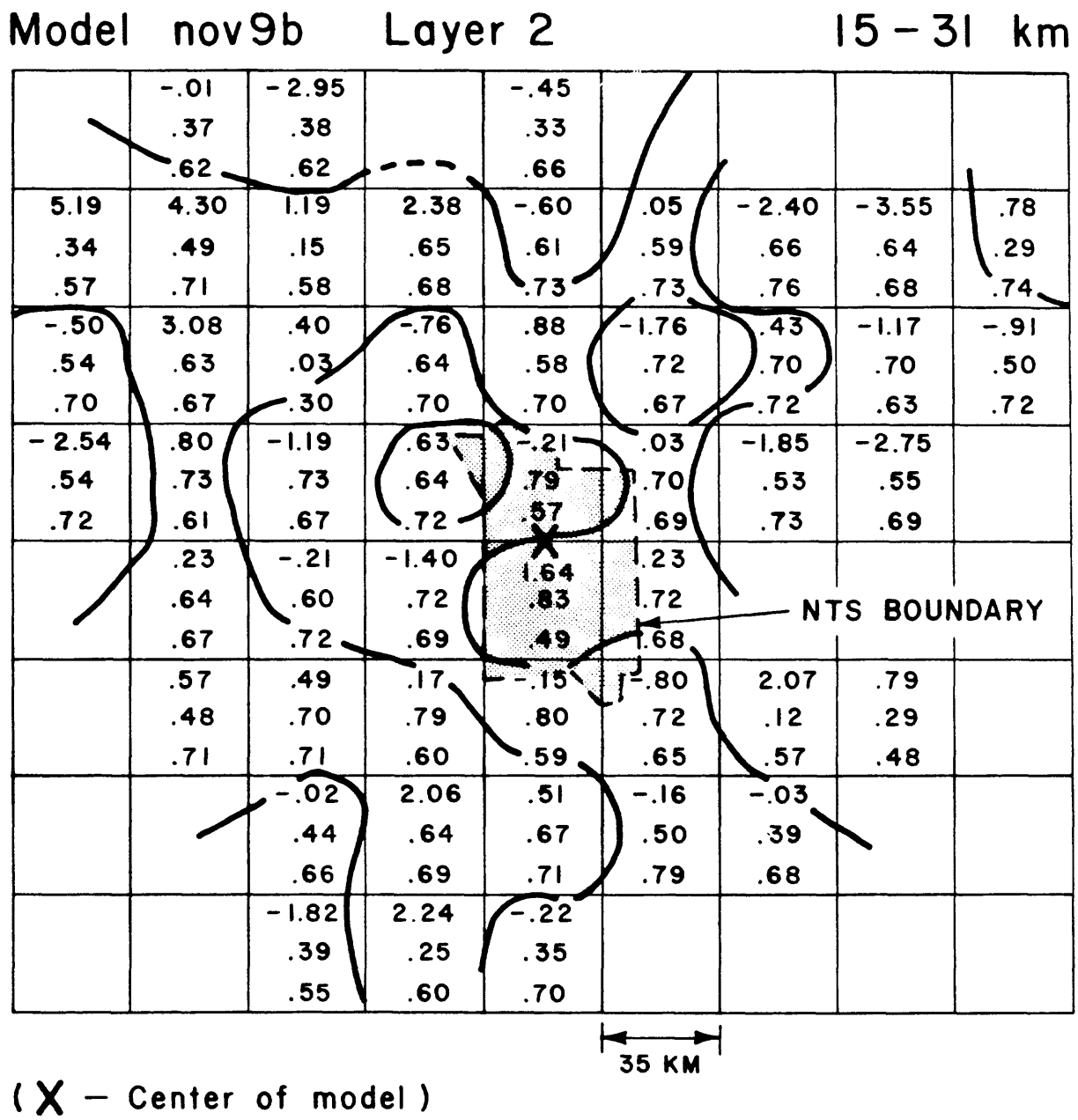

Figure 10. Model nov9b in (a) layer 2, (b) layer 3, (c) layer 4, and (d) layer 5. Layer 1 is shown in Figure 9. Zero perturbation contours are shown. In each block the top number is the velocity perturbation, the middle number is the diagonal element of the resolution matrix, and the bottom number is the standard error for the block. Blocks without numbers did not have enough rays to be modeled. The center of the model, indicated by the heavy "X," is at station BGB; NTS is shaded. Comparison with Figures 1 and 8 provides the necessary geographic reference.

Model nov9b Layer 3 31 - 81 km

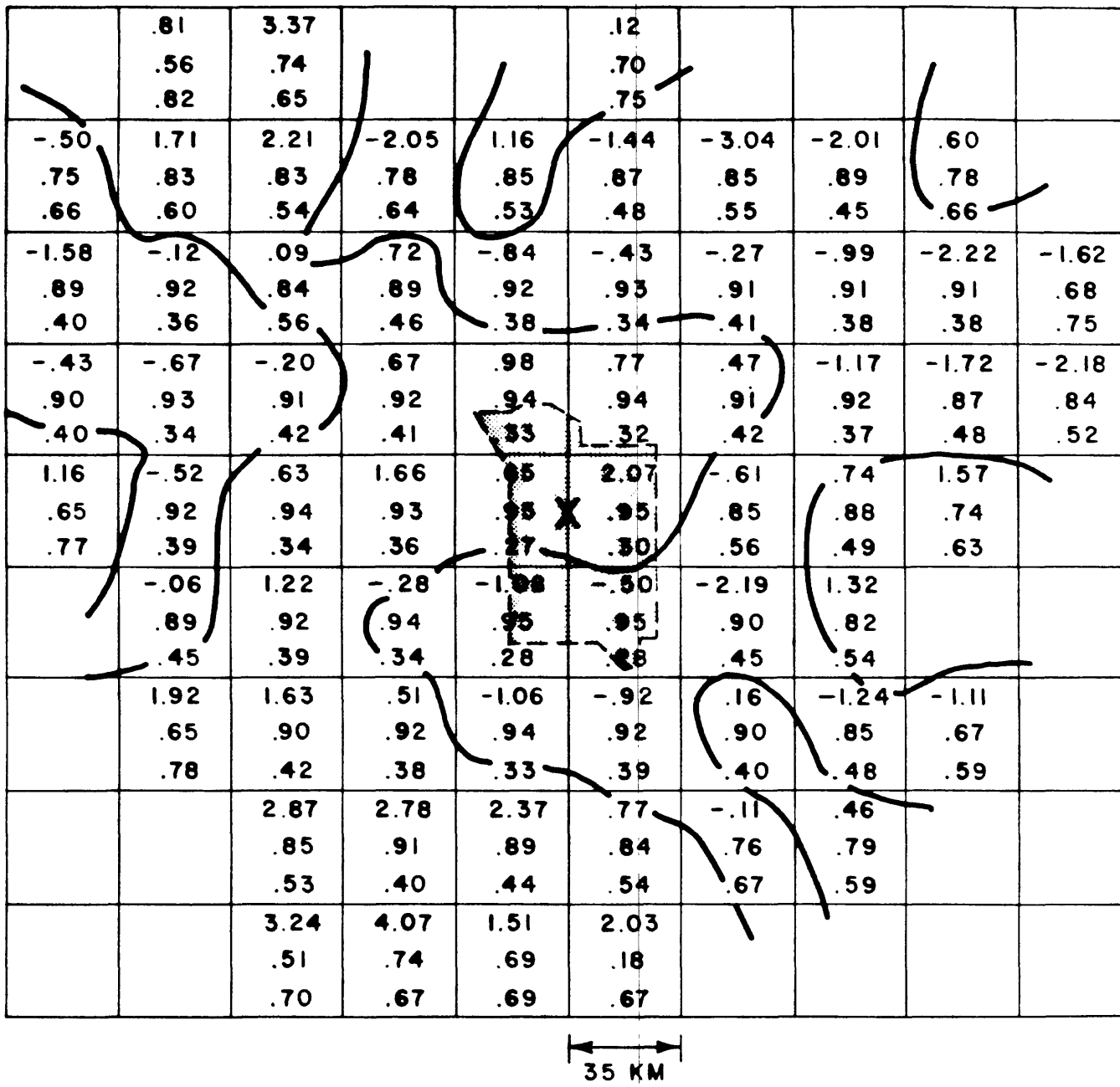

Figure 10b

Model nov9b Layer 4 81 - 131 km

	1.07 .72 .73		.40 .76 .71	.68 .70 .72	-1.88 .79 .62	-2.36 .80 .62	1.43 .77 .71		
-.74 .85 .62	.30 .83 .58	-1.30 .85 .54	-1.46 .86 .54	1.50 .87 .49	2.78 .87 .50	-.03 .89 .46	-.69 .87 .49	1.18 .75 .67	
-1.16 .92 .46	-.44 .89 .49	-.16 .91 .44	1.29 .92 .40	3.90 .92 .41	1.37 .91 .43	-.77 .92 .40	-1.00 .89 .48	-1.41 .85 .56	-1.01 .74 .74
1.59 .93 .42	-1.08 .89 .47	-.98 .93 .37	1.21 .94 .35	4.03 .93 .36	3.60 .93 .35	.60 .92 .39	-.54 .91 .41	-1.30 .84 .56	1.59 .89 .52
1.44 .88 .51	-.15 .90 .46	.96 .94 .36	1.38 .94 .34	3.37 .94 .32	2.96 .93 .36	-.18 .92 .39	-.84 .88 .51	-.36 .81 .63	1.64 .85 .57
1.08 .74 .74	.93 .88 .51	.28 .91 .43	1.62 .94 .35	.81 .94 .32	-.66 .93 .35	-2.17 .92 .40	-1.88 .84 .58	-1.72 .80 .61	.24 .67 .74
	.82 .84 .56	1.37 .90 .46	.97 .93 .35	-.72 .93 .36	-1.64 .93 .37	-2.27 .90 .43	-3.97 .78 .62	.74 .53 .83	
	1.10 .77 .71	.45 .83 .59	1.99 .87 .54	-.85 .89 .47	-.18 .89 .47	-1.23 .82 .60	-1.40 .81 .61	-.05 .62 .77	-1.00 .69 .69
		1.37 .68 .66	1.49 .69 .74	.01 .75 .64	1.14 .75 .67	.25 .64 .70			

35 KM

Figure 10c

Model nov9b Layer 5 131 - 231 km

-.82 .88 .51	.46 .85 .63	2.05 .89 .51	2.59 .86 .60	3.74 .91 .45	3.36 .89 .50	2.70 .88 .54			
-.02 .95 .39	-.72 .94 .40	1.48 .94 .42	.67 .95 .36	.75 .95 .35	1.69 .96 .33	1.24 .96 .32	4.19 .93 .42	-.87 .89 .53	-1.33 .87 .57
-.37 .97 .30	-.41 .96 .32	.00 .97 .29	-.22 .97 .28	1.61 .97 .28	1.93 .96 .29	1.90 .97 .28	1.11 .95 .33	.67 .86 .59	.16 .91 .48
.74 .97 .28	.35 .97 .27	.05 .98 .23	-.04 .98 .23	2.26 .97 .25	2.54 .97 .25	.86 .97 .24	.81 .96 .31	-.53 .94 .39	.28 .85 .61
2.34 .97 .28	1.53 .98 .25	1.25 .98 .24	.38 .99 .17	1.88 .98 .21	1.30 .97 .26	-.54 .98 .21	-1.52 .96 .30	.33 .94 .40	-.44 .95 .37
2.84 .97 .27	2.02 .97 .29	.55 .98 .25	-.19 .98 .19	.28 .98 .19	-.13 .98 .23	-1.62 .98 .21	-1.55 .96 .30	-1.61 .95 .35	-.91 .95 .36
1.47 .96 .32	.84 .97 .27	.97 .98 .24	-.37 .98 .18	-.57 .98 .21	-1.29 .98 .23	-2.06 .97 .25	-1.04 .96 .31	-1.04 .96 .32	-.61 .89 .52
.08 .96 .32	.42 .95 .35	.07 .97 .26	-.79 .98 .21	-1.37 .98 .22	-1.10 .97 .27	-.96 .98 .23	-.60 .95 .36	.02 .95 .37	-.95 .85 .61
-.49 .86 .60	.67 .93 .42	.21 .96 .31	-1.00 .97 .26	-.95 .97 .28	-.69 .97 .27	-.01 .97 .28	.73 .95 .36	-.86 .93 .41	-.54 .87 .54
	.87 .95 .40	.08 .93 .41	-.90 .96 .32	.02 .94 .38	.93 .94 .39	1.10 .95 .36	.19 .92 .43	-1.70 .93 .40	-1.62 .85 .57
		-.47 .65 .77	-1.25 .76 .75	.75 .89 .49	2.15 .78 .65	.15 .87 .56	-.62 .85 .57	-1.35 .85 .61	-1.21 .84 .64

35 KM

Figure 10d

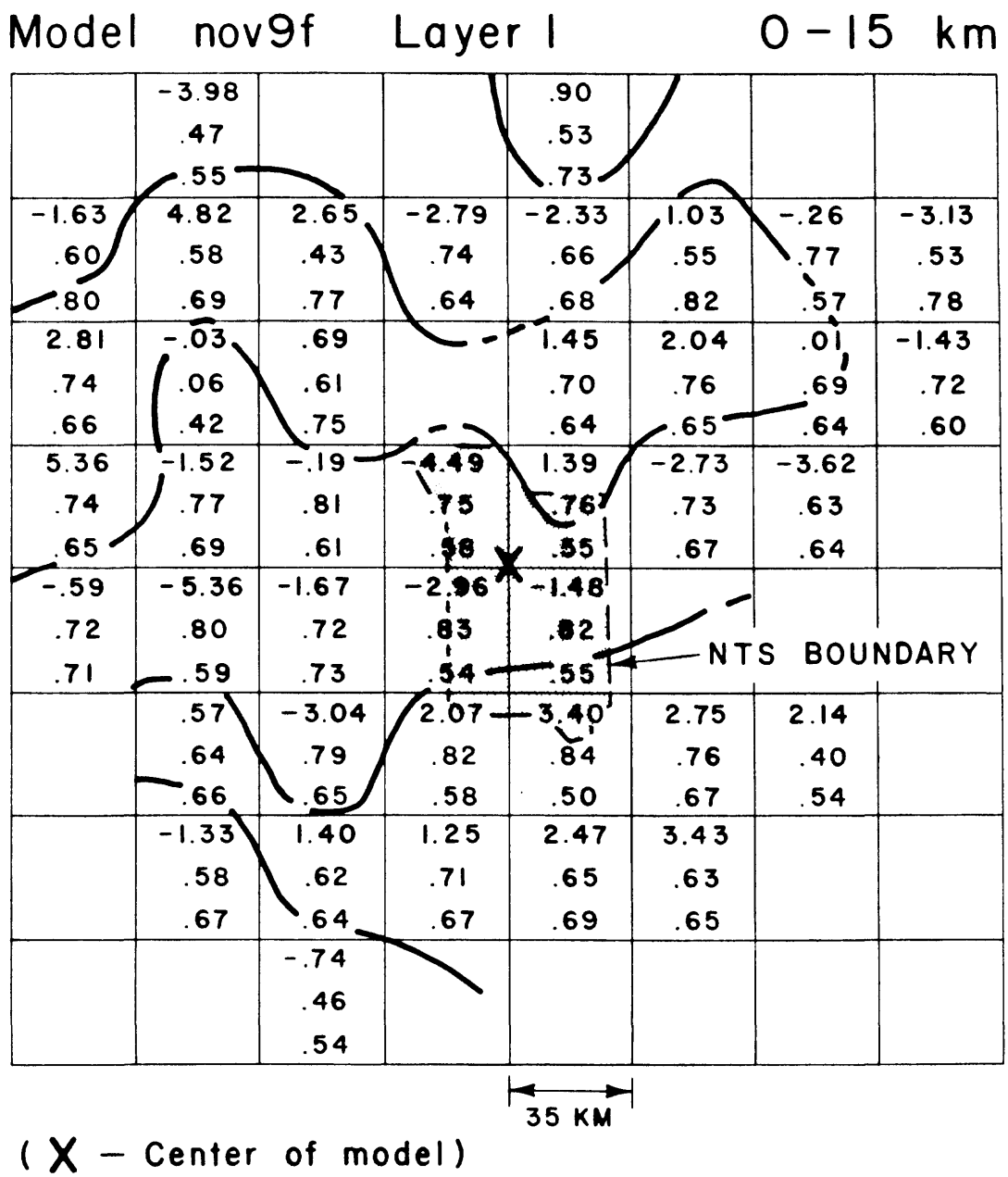

Figure 11. Model nov9f for (a) layer 1, (b) layer 2, (c) layer 3, (d) layer 4, and (e) layer 5. Format is the same as in Figure 10. The starting model is the same as that of nov9b except that the upper layer of nov9f was divided into blocks rather than being modeled as station corrections.

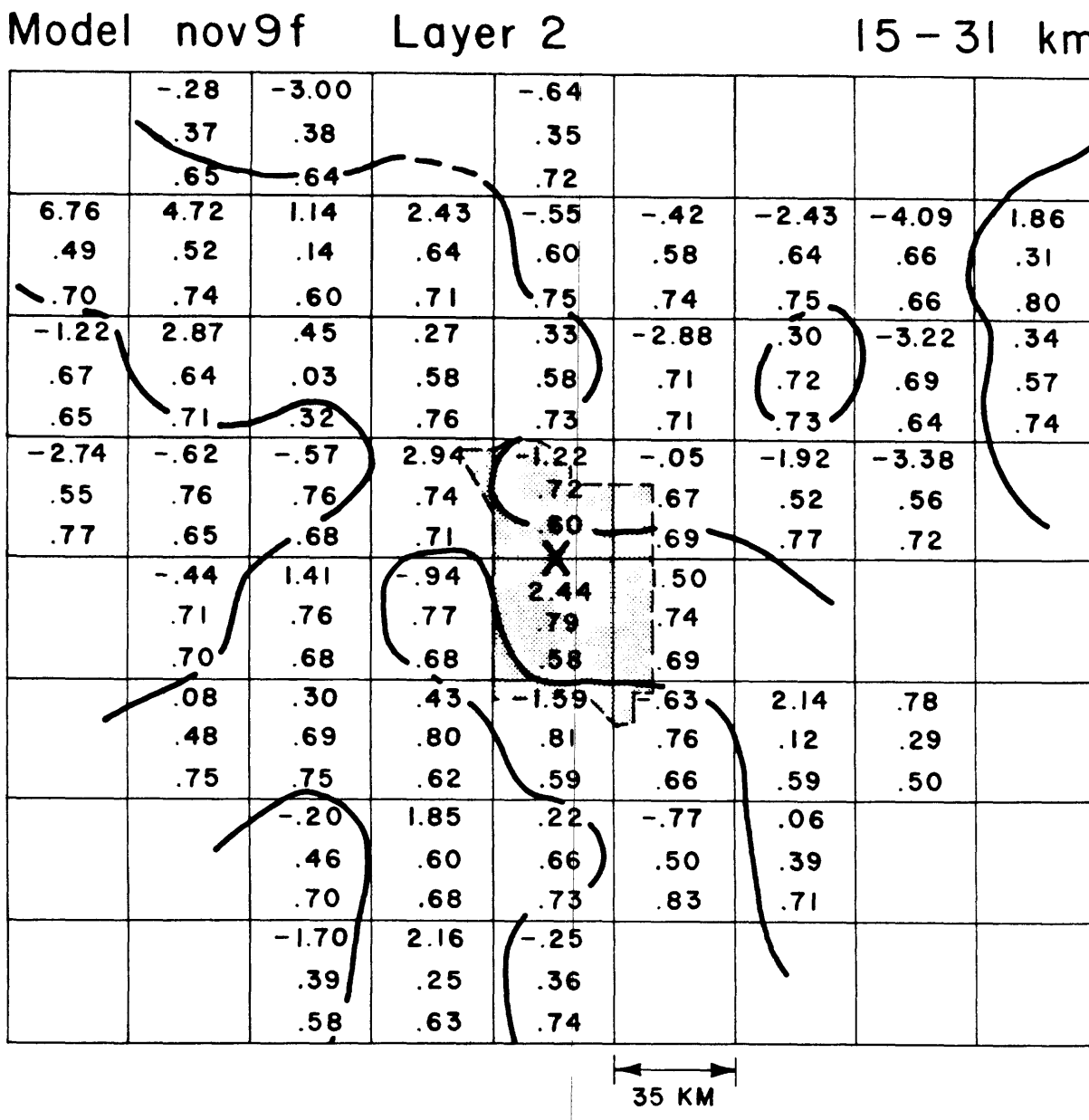
Model nov9f Layer 2
15 - 31 km
-.28
-3.00
-.64
.37
.38
.35
.65
.64
.72
6.76
4.72
1.14
2.43
-.55
-.42
-2.43
-4.09
1.86
.49
.52
.14
.64
.60
.58
.64
.66
.31
.70
.74
.60
.71
.75
.74
.75
.66
.80
-1.22
2.87
.45
.27
.33
-2.88
.30
-3.22
.34
.67
.64
.03
.58
.58
.71
.72
.69
.57
.65
.71
.32
.76
.73
.71
.73
.64
.74
-2.74
-.62
-.57
2.94
-1.22
-.05
-1.92
-3.38
.55
.76
.76
.74
.72
.67
.52
.56
.77
.65
.68
.71
.60
.69
.77
.72
-.44
1.41
-.94
2.44
1.50
.71
.76
.77
.79
.74
.70
.68
.68
.58
.69
.08
.30
.43
-1.59
-.63
2.14
.78
.48
.69
.80
.81
.76
.12
.29
.75
.75
.62
.59
.66
.59
.50
-.20
1.85
.22
-.77
.06
.46
.60
.66
.50
.39
.70
.68
.73
.83
.71
-1.70
2.16
-.25
.39
.25
.36
.58
.63
.74
35 KM

Figure 11b

Model nov9f Layer 3 31-81 km

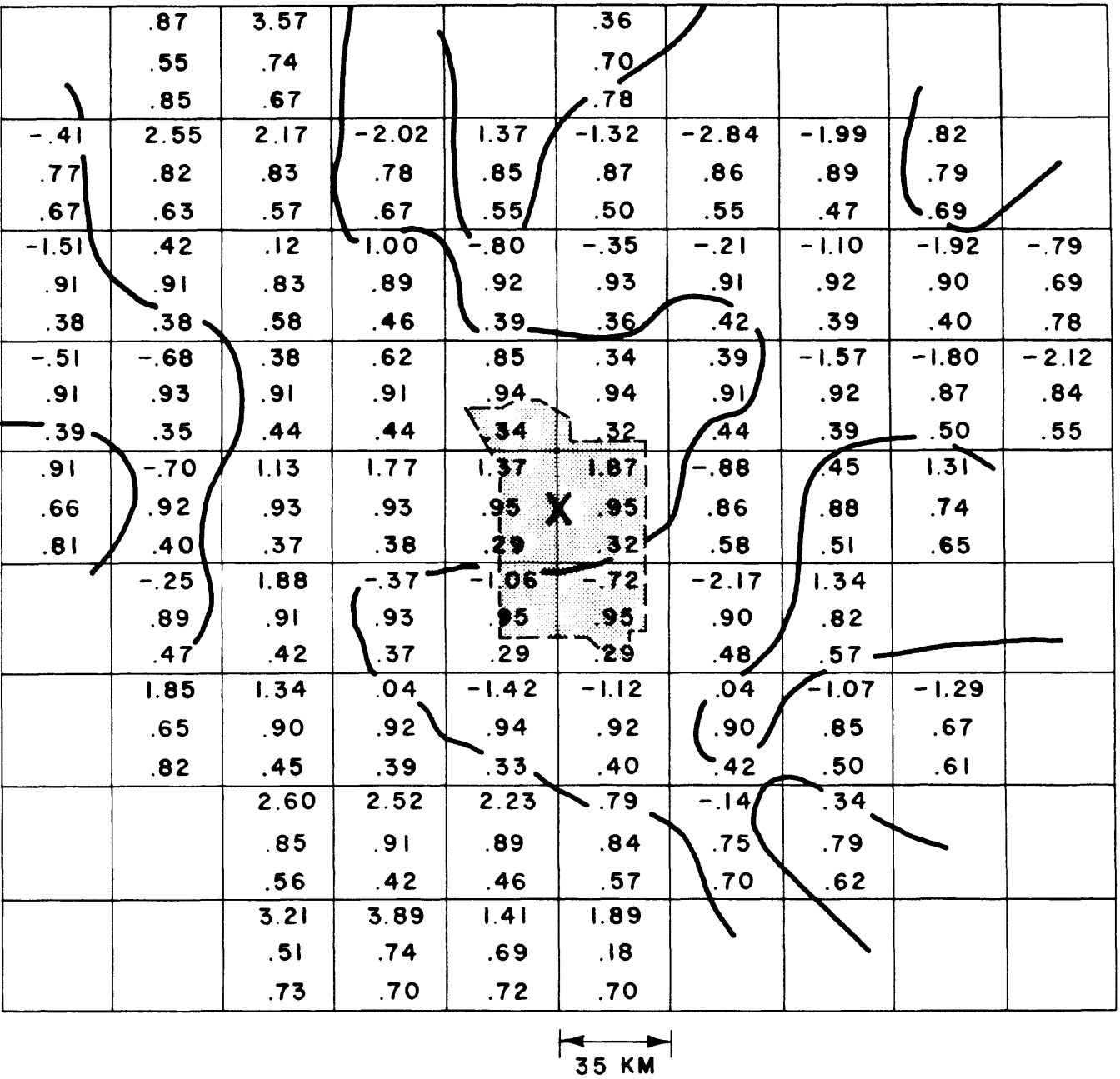

Figure 11c

Model nov9f Layer 4 81 – 131 km

	1.02 .72 .75		.48 .76 .74	.75 .70 .75	-1.77 .79 .64	-2.39 .80 .65	1.73 .77 .74		
-.48 .85 .64	.14 .83 .60	-1.10 .85 .57	-1.48 .86 .56	1.60 .87 .51	2.93 .87 .52	0.00 .89 .48	-.28 .88 .51	1.29 .77 .70	
-1.28 .92 .48	-.42 .88 .52	-.15 .91 .46	1.38 .92 .41	3.77 .92 .43	1.33 .91 .45	-.78 .92 .41	-.87 .89 .50	-1.38 .85 .58	-.62 .75 .77
1.58 .93 .44	-.55 .89 .49	-.87 .93 .39	1.52 .94 .37	4.53 .93 .37	4.02 .94 .36	.65 .92 .40	-.47 .91 .43	-.70 .85 .57	1.53 .90 .53
1.47 .88 .53	-.09 .90 .47	.78 .94 .37	.80 .94 .35	3.06 .94 .33	2.95 .94 .37	-.17 .92 .41	-.79 .88 .53	-.59 .81 .66	1.55 .84 .59
.80 .74 .77	.89 .88 .53	.14 .91 .45	1.53 .94 .36	.70 .94 .33	-.42 .93 .37	-2.14 .92 .41	-2.13 .84 .61	-1.81 .80 .64	.23 .67 .77
	.82 .84 .59	1.75 .90 .48	1.28 .93 .36	-.66 .93 .37	-1.61 .93 .38	-2.74 .91 .45	-4.02 .79 .65	.63 .53 .86	
	1.22 .77 .74	.69 .83 .62	2.09 .86 .56	-.93 .89 .49	-.30 .89 .49	-1.49 .82 .62	-1.61 .82 .63	-.28 .62 .80	-1.06 .69 .72
		1.27 .68 .69	1.54 .69 .77	-.05 .75 .67	1.07 .76 .69	.11 .64 .73			

35 KM

Figure 11d

Model nov9f Layer 5 131 – 231 km

-.74	.51	2.16	2.49	3.86	3.45	2.93			
.88	.85	.89	.86	.91	.90	.88			
.53	.65	.53	.62	.46	.52	.56			
.08	-.88	1.63	.62	.72	1.74	1.29	4.12	-.85	-1.35
.95	.94	.94	.95	.95	.96	.96	.93	.89	.87
.41	.42	.44	.38	.37	.34	.34	.44	.55	.60
-.39	-.18	-.22	-.14	1.54	1.91	1.86	1.09	.75	.14
.97	.96	.97	.97	.97	.97	.97	.95	.85	.91
.31	.34	.30	.29	.29	.30	.29	.35	.61	.50
.85	.03	.29	-.11	2.51	2.56	.81	.88	-.58	.10
.97	.97	.98	.98	.97	.97	.97	.96	.94	.85
.29	.28	.24	.24	.26	.26	.25	.33	.41	.64
2.34	1.51	1.22	.49	1.77	1.30	-.46	-1.37	.15	-.41
.97	.98	.98	.99	.98	.97	.98	.96	.94	.95
.29	.26	.25	.18	.21	.27	.22	.31	.41	.39
2.95	2.03	.55	-.26	.37	-.25	-1.58	-1.55	-1.55	-.87
.97	.97	.98	.98	.98	.98	.98	.96	.95	.95
.28	.30	.26	.20	.20	.24	.22	.31	.37	.37
1.55	.93	.93	-.12	-.31	-1.24	-2.17	-1.09	-.91	-.39
.96	.97	.98	.98	.98	.98	.97	.96	.96	.89
.33	.28	.25	.19	.22	.22	.26	.32	.34	.54
.15	.29	-.04	-.82	-1.37	-1.22	-.86	-.15	-.09	-.97
.96	.95	.97	.98	.98	.97	.98	.95	.95	.85
.34	.37	.27	.22	.23	.28	.24	.38	.38	.64
-.49	.62	.14	-.92	-.88	-.57	-.03	.83	-1.02	-.29
.86	.93	.96	.97	.97	.97	.97	.95	.93	.87
.62	.44	.32	.27	.29	.28	.29	.37	.43	.57
	.84	.06	-.92	-.01	.83	1.01	.23	-1.67	-1.49
	.95	.93	.96	.94	.94	.95	.92	.93	.85
	.41	.43	.34	.39	.40	.38	.45	.42	.59
		-.56	-1.43	.74	2.22	.09	-.55	-1.64	-1.33
		.65	.76	.89	.78	.87	.85	.85	.84
		.81	.78	.51	.67	.59	.59	.63	.67

35 KM

Figure 11e

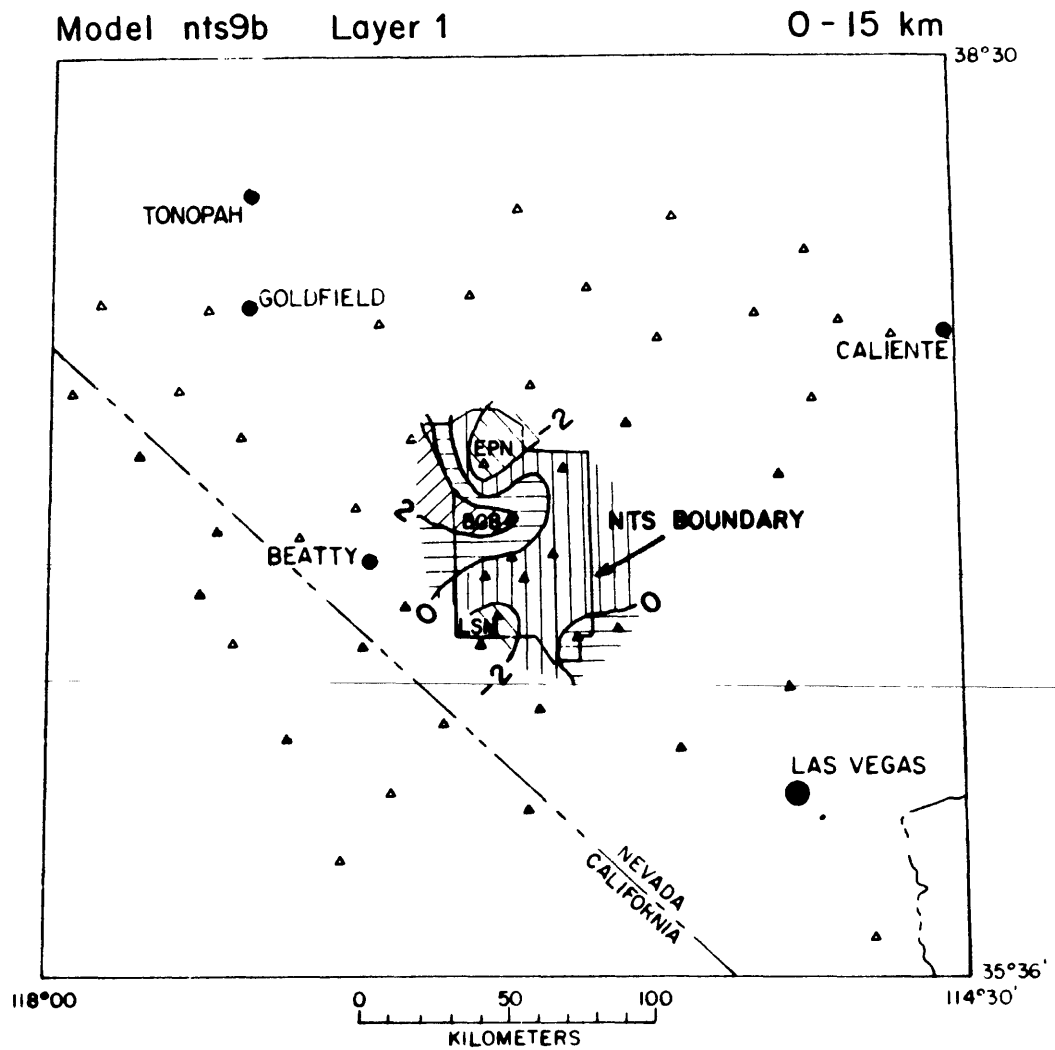

Figure 12. Upper layer of model nts9b modeled as station corrections. See Figure 9 for explanation of format.

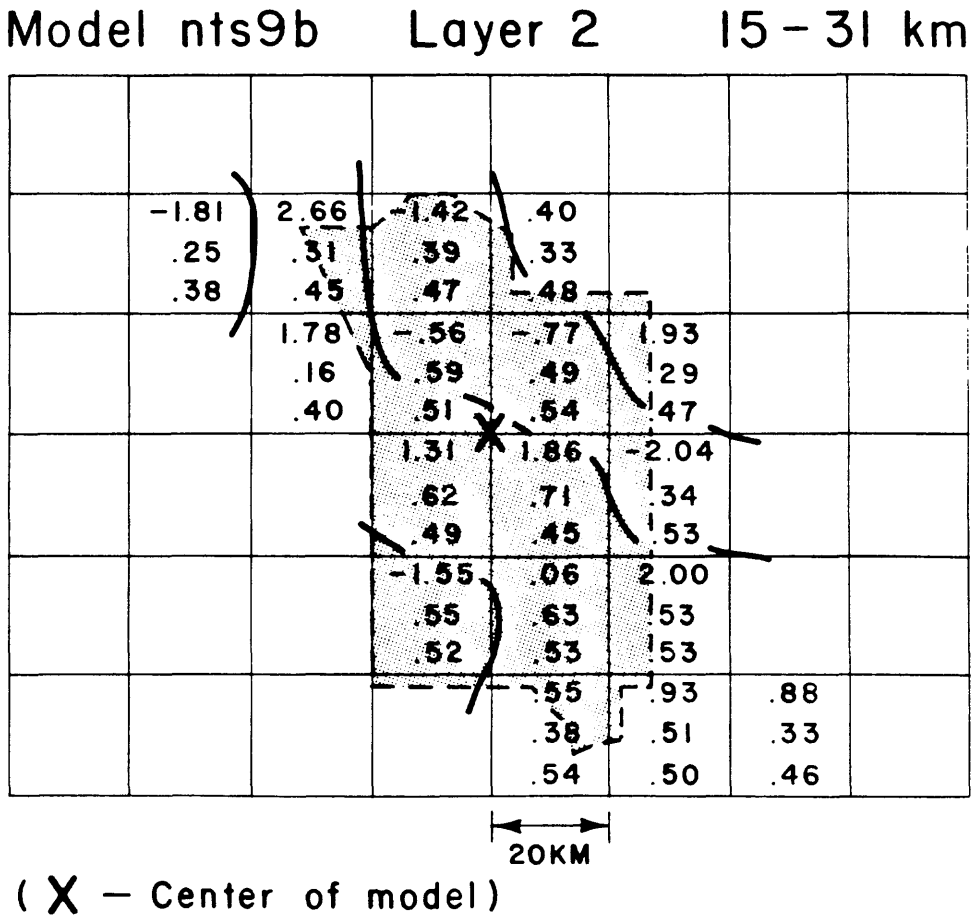

Figure 13. Deeper layers of model nts9b: (a) layer 2, (b) layer 3, (c) layer 4, and (d) layer 5. Block size is smaller than in model nov9b to make use of the denser network coverage around NTS. Format is the same as in Figure 10.

Model nts9b Layer 3 31 - 81 km

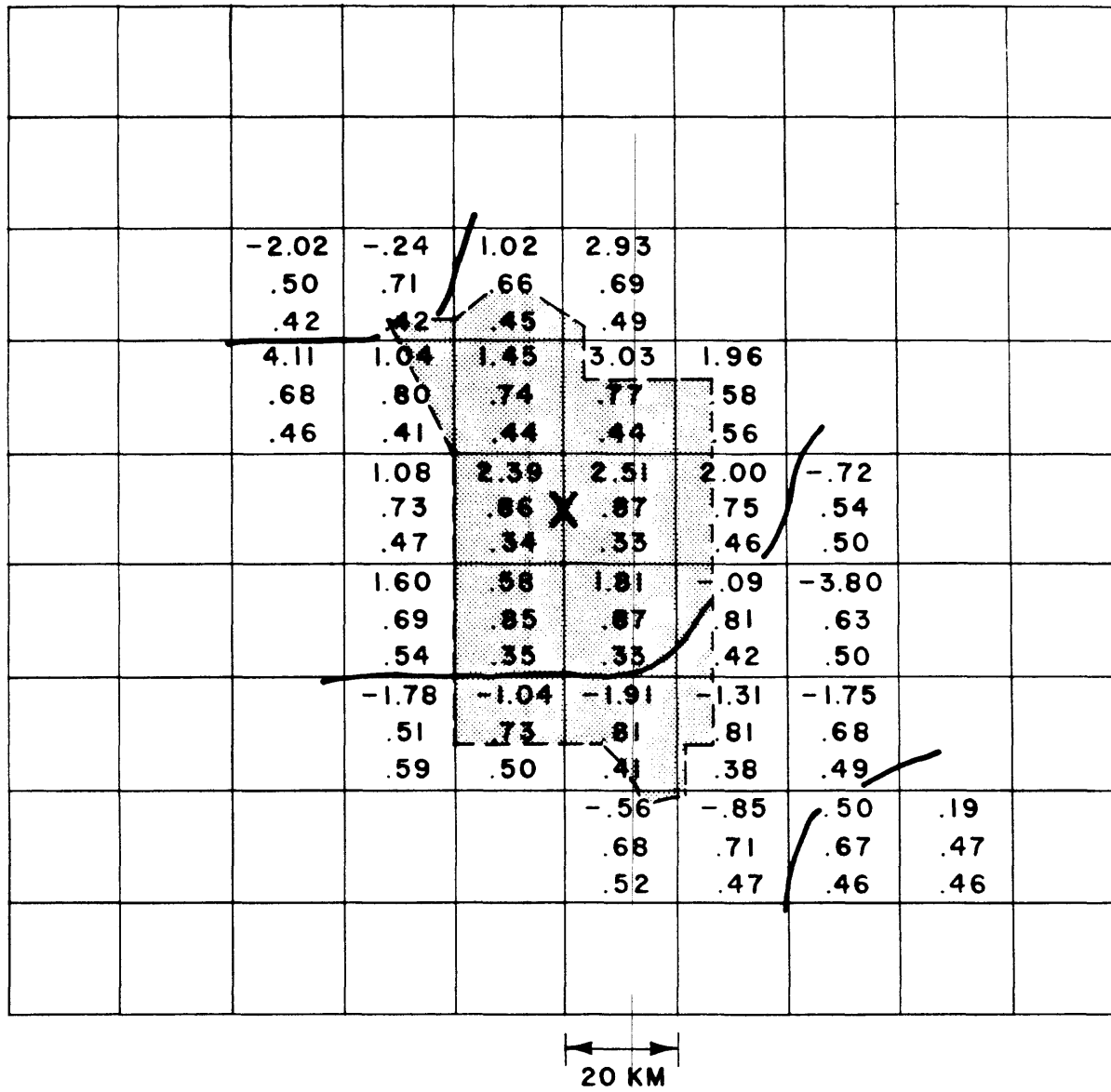

Figure 13b

Model nts9b Layer 4 81 – 131 km

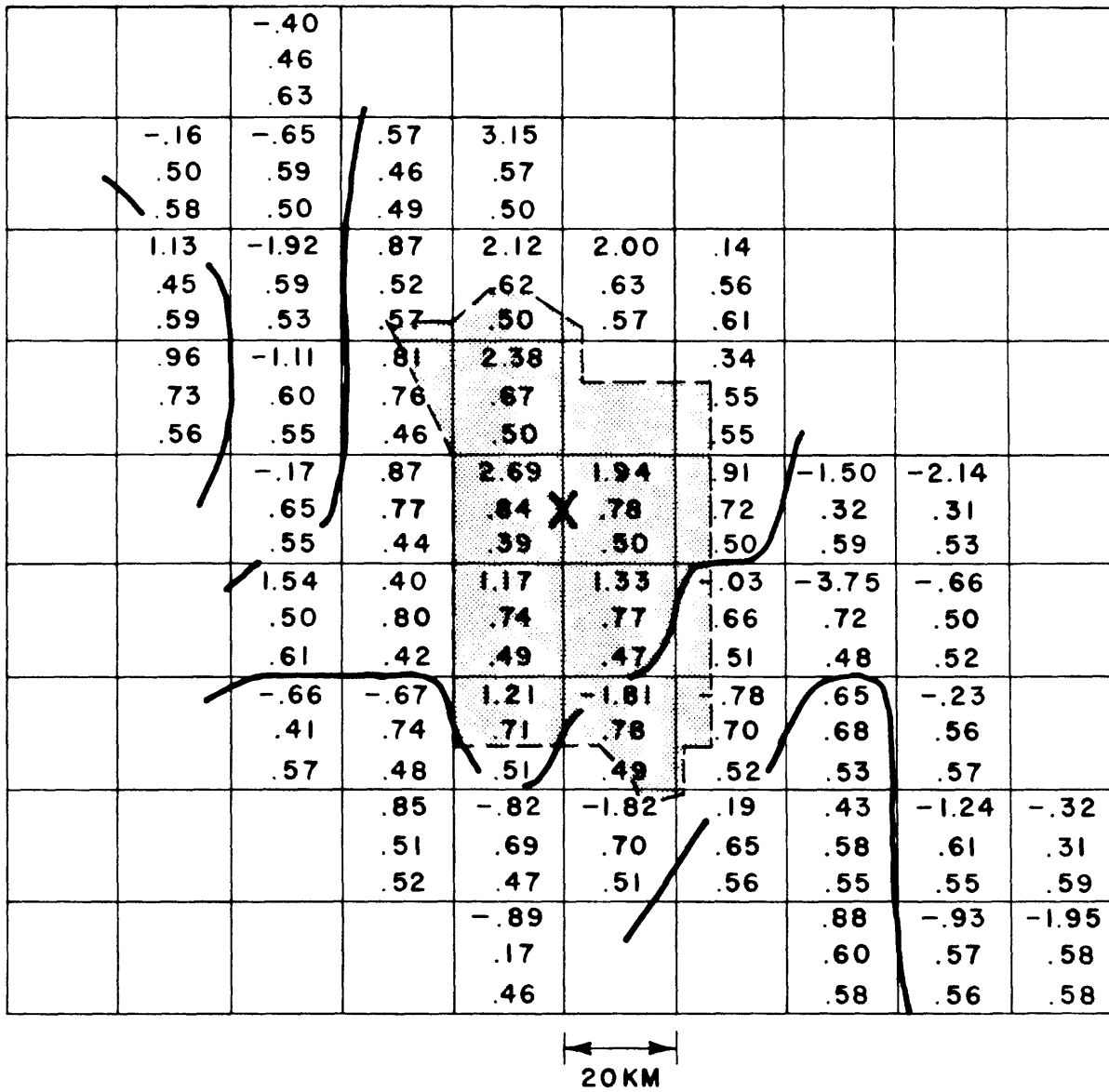

Figure 13c

Model nts9b Layer 5 131 – 231 km

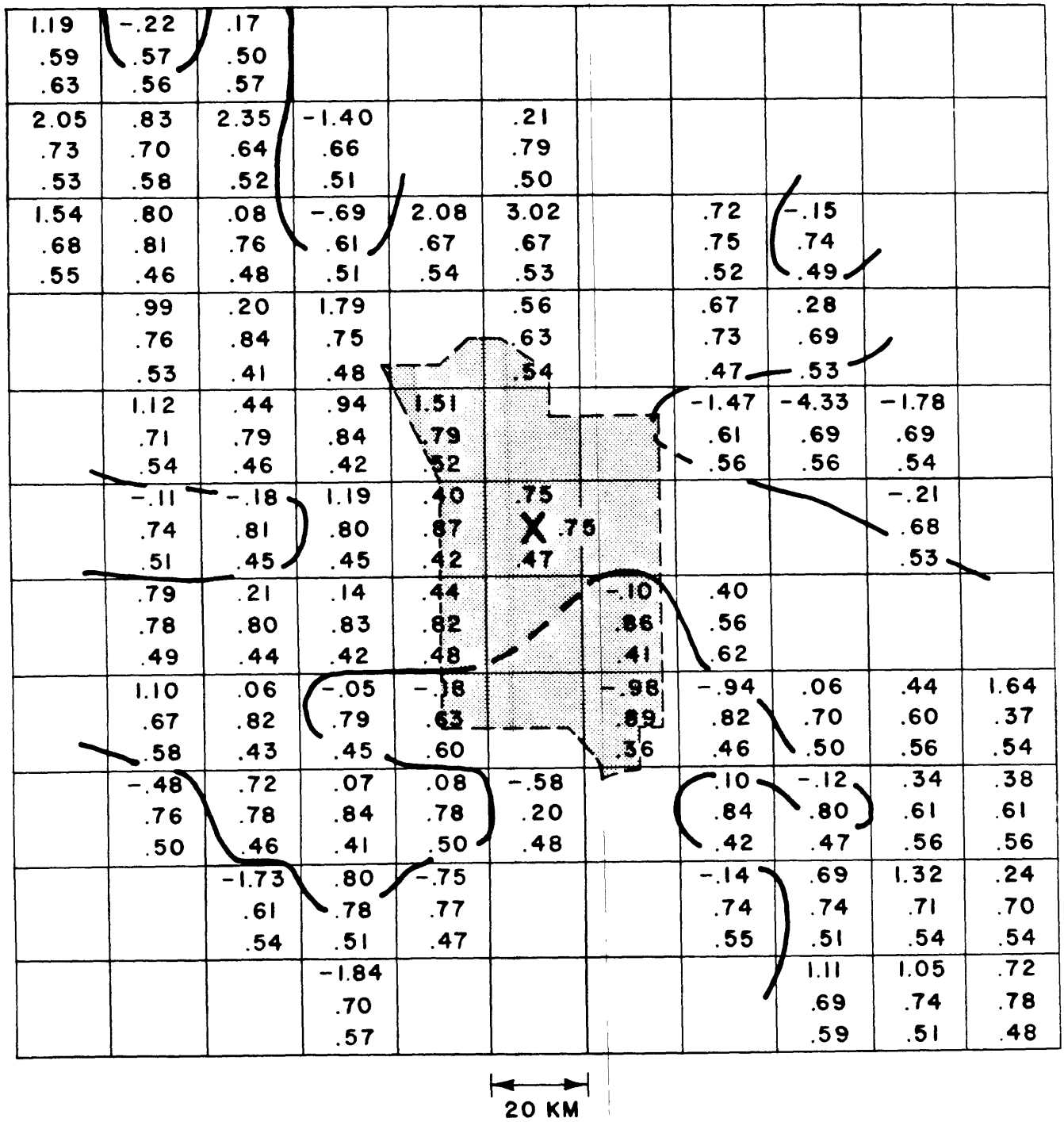

Figure 13d